SPECIAL TOPIC

Ion cyclotron emission measurements during JET deuterium-tritium experiments

ION CYCLOTRON EMISSION MEASUREMENTS DURING JET DEUTERIUM-TRITIUM EXPERIMENTS

G.A. COTTRELL, V.P. BHATNAGAR, O. DA COSTA, R.O. DENDY[+], J. JACQUINOT, K.G. McCLEMENTS[+], D.C. McCUNE[++], M.F.F. NAVE*, P. SMEULDERS, D.F.H. START
JET Joint Undertaking, Abingdon, Oxfordshire, United Kingdom
[+]AEA Technology, Fusion, Culham Laboratory, Abingdon, Oxfordshire, United Kingdom (Euratom/UKAEA Fusion Association)
[++]Princeton Plasma Physics Laboratory, Princeton University, Princeton, New Jersey, United States of America
*Associacão IST/Euratom, Centro de Fusão Nuclear, Instituto Superior Téchnico, Lisbon, Portugal and Labóratorio Nacional de Engenharia e Technologia Industrial, Lisbon, Portugal

ABSTRACT. In the course of the Preliminary Tritium Experiment in JET, where combined deuterium and tritium neutral beam injection generated a DT fusion power of 1.7 MW, ion cyclotron emission (ICE) was measured in the frequency range $\nu \leq 180$ MHz. The ICE spectra contain superthermal, narrow, equally spaced emission lines, which correspond to successive cyclotron harmonics of deuterons or alpha particles at the outer midplane, close to the last closed flux surface at major radius $R \sim 4.0$ m. Above about 100 MHz the lines merge into a relatively intense continuum. The ICE signal fluctuates rapidly in time, and is extinguished whenever a large amplitude edge localized mode (ELM) occurs. In pure deuterium and mixed DT discharges ICE spectra are similar in form, but on changing from pure D to mixed D + T neutral beam injection at constant power, the intensity of the ICE rises in proportion to the increased neutron flux: this indicates that fusion alpha particles — and not beam ions — provide the free energy to generate ICE. The JET ICE database, which now extends over a range of six decades in signal intensity, shows that the time averaged ICE power increases almost linearly with total neutron flux. The rise and fall of the neutron flux during a single discharge is closely followed by that of the ICE signal, which is delayed by a time of the order of the fusion product slowing down time. This feature is well modelled by a TRANSP code simulation of the density of deeply trapped fusion products reaching the plasma edge. Calculations reveal a class of fusion products, born in the core, which make orbital excursions of sufficient size to reach the outer midplane edge. There, the velocity distribution has a ring structure, which is found to be linearly unstable to relaxation to obliquely propagating waves on the fast Alfvén-ion Bernstein branch at all ion cyclotron harmonics. The paper shows how ICE provides a unique diagnostic for fusion alpha particles.

1. INTRODUCTION

The original motivation for measuring ion cyclotron emission (ICE) from a large, hot, dense tokamak plasma, such as that produced in JET [1] (major radius $R = 2.96$ m, minor radius $a = 1.2$ m), arose from the possibility of observing optically thick harmonic emission from the thermal ions. However, in JET deuterium plasmas, it has been found that the confined superthermal population of charged fusion products radiates strongly at ion cyclotron frequencies [2]. Thus ICE observations offer a possible method for measuring the characteristics of energetic charged particles in magnetic fusion experiments. We recall that in pure deuterium plasmas, the following primary fusion reactions take place with equal probability:

$$D + D \rightarrow {}^3He(0.82\ MeV) + n(2.45\ MeV) \quad (1)$$

$$D + D \rightarrow T(1.0\ MeV) + p(3.0\ MeV) \quad (2)$$

In addition, secondary reactions can take place between the energetic products of fusion reactions (1) and (2) and the deuterons,

$$^3He + D \rightarrow p(14.6\ MeV) + {}^4He(3.7\ MeV) \quad (3)$$

$$T + D \rightarrow {}^4He(3.6\ MeV) + n(14.0\ MeV) \quad (4)$$

For deuterium-tritium (DT) plasmas in the ion temperature regimes of present tokamak experiments ($T_i \sim$ 10–20 keV), fusion reaction (4) is dominant by virtue of the relatively large ratio of DT to DD cross-sections.

Ion cyclotron emission has previously been observed in a number of pure deuterium fuelled tokamaks at frequencies $\nu \leq 500$ MHz, and we begin by reviewing the data obtained. On the TFR tokamak [3], superthermal ICE from the peripheral region of the plasma was found. A similar result [4] was found on the JET tokamak, where the ICE spectra showed narrow ($\Delta\nu/\nu \sim 0.1 \ll a/R \sim 0.4$) superthermal emission

lines, superimposed on a broad background continuum, with regular spacing proportional to the magnetic field. These observations confirm the cyclotronic character of the emission, and further indicate that the detected ICE originates from a localized region of radial extent $\Delta R \cong 20$ cm. In JET ohmically heated deuterium discharges [2], the intensity of the ICE lines increased linearly with the DD fusion reaction rate over three orders of magnitude in signal intensity, indicating that charged fusion products provide the free energy to drive ICE. By applying frequency matching considerations to JET ICE data [5], it was shown that the frequencies of the emission lines coincide uniquely with harmonics, l, of the deuteron (degenerate with the alpha particle) gyrofrequency, evaluated in the total field at the position of the outer midplane edge: $\omega = l\Omega_D = l\Omega_\alpha$, where Ω_D and Ω_α are, respectively, the gyrofrequencies of the bulk deuterons and alpha particles. The signals apparently originated in the near field region of the detecting ICRH antenna on JET. In addition, time resolved ICE signals on JET high current ohmically heated discharges correlated with inverted sawteeth [6], seen in data from edge soft X ray and D_α diagnostics.

Ion cyclotron emission measurements have also been made on the TFTR tokamak using RF probes mounted above the plasma [7]. With deuterium neutral beam injection (NBI), the spectra showed cyclotron harmonic peaks with frequencies corresponding to the edge $\omega = l\Omega_D = l\Omega_\alpha$, a result in qualitative agreement with the JET results. However, in ohmically heated discharges, a different set of lines was seen with frequencies related to the odd deuteron harmonics: $\omega = (l + 1/2)\Omega_H$. Thus lines with frequencies $\omega = l\Omega_D (l = 2, 4, 6, \ldots)$, seen in JET Ohmic data, were apparently missing from the TFTR data. Although this difference is not understood, both sets of data point to localization of the cyclotron harmonic emission at the outer midplane edge of the tokamak. At higher frequencies ($100 \lesssim \nu \lesssim 350$ MHz), a broadband feature was found in the TFTR data, peaking at a frequency of $\nu \sim 150$ MHz. The intensity of this feature was found to follow the time evolution of the neutron emission. More recent observations [8] with deuterium NBI on TFTR show emission lines that correspond to the edge ion cyclotron harmonics of ^{3}He ions, in addition to those of the deuterons. Such ions could be produced by fusion reaction (1).

In summary, there is strong experimental evidence that a minority fusion product population in a deuterium plasma can excite superthermal ICE with spectral peaks at multiple cyclotron harmonics in the outer midplane edge of a tokamak plasma. The aim of the present series of measurements on JET was to acquire new data to provide a better understanding of the ICE mechanism which, in turn, is important in assessing the potential of ICE as a diagnostic for confined energetic fusion alpha particles in DT plasmas. The JET Preliminary Tritium Experiment (PTE) [9] therefore offered an ideal opportunity to monitor ICE from a large tokamak plasma in which the fusion product population was dominated by energetic alpha particles, produced by reaction (4), and not by the products of pure deuterium fusion reactions. Some preliminary data on the PTE ICE experiment have already been reported [10]. However, in this paper, a more comprehensive analysis of the experimental data and discussion of possible models is presented. A description of the experimental method appears in Section 2, together with an assessment of the experimental uncertainties. Section 3 contains the results of the ICE measurements: these include power spectra for pure deuterium and mixed DT NBI heated discharges, the relationship between the ICE power detected and the alpha particle content of the plasma determined with the TRANSP [11] Monte Carlo model, and a comparison of the time evolution of ICE with the alpha particle content of the DT plasma. The correlation between ICE signals and MHD events — sawteeth and edge localized modes (ELMs) — is also described. Section 4 summarizes the general properties and status of the ICE data and the challenge that these present to theoretical models of the emission mechanism. Calculations of the structure of the energetic ion distribution are presented in Section 5, showing the existence of a class of trapped particles which are born close to the centre but intercept the outer edge plasma, contributing to a ring velocity distribution which is anisotropic, radially inhomogeneous and not monotonically decreasing. We show that ion cyclotron instability leads to simultaneous excitation of the quasi-perpendicular fast Alfvén-ion Bernstein wave at cyclotron harmonics $l\Omega_\alpha (l = 1, \ldots, 10)$ of the energetic ions, for parameters appropriate to the JET tritium discharges. Section 6 contains a discussion of the results and Section 7 the conclusions.

2. EXPERIMENTAL METHOD

In the PTE series of NBI heated hot ion H mode discharges [9], the plasma was configured as a single null X point discharge, with reversed toroidal field so that the ion ∇B drift was directed away from the upper dump plates. The PTE series contained dis-

TABLE I. JET PTE DT PARAMETERS: (PULSE No. 26148 AT TIME OF 13.2 s)

Plasma current, I_p	3.1 MA
Toroidal field, B_T	2.8 T
Central electron density, $n_e(0)$	3.6×10^{19} m^{-3}
Injected D neutral beam power	12.8 MW
Injected T neutral beam power	1.5 MW
*Central D + T ion density, $n_i(0)$ (thermal)	2.0×10^{19} m^{-3}
*Ratio: average T to average D + T density (thermal)	0.103
Central electron temperature, $T_e(0)$	9.9 keV
Central ion temperature, $T_i(0)$	18.0 keV
Diamagnetic stored energy	9.1 MJ
Total neutron flux	6×10^{17} s^{-1}
Fusion power	1.7 MW
Central Larmor radius of 3.6 MeV alpha particle, $\rho_\alpha(0)$	9.7 cm
Central Alfvén velocity, $c_A(0)$	7.08×10^6 ms^{-1}
Alpha particle birth velocity, $v_{\alpha 0}$	1.3×10^7 ms^{-1}
$v_{\alpha 0}/c_A(0)$	1.8
*Volume averaged toroidal alpha particle beta, $\langle\beta_\alpha\rangle$	1.36×10^{-4}
*Central toroidal alpha particle beta, $\beta_\alpha(0)$	1.07×10^{-3}
*$n_\alpha(0)/n_e(0)$	6.5×10^{-4}
*Central alpha particle slowing down time, $\tau_\alpha(0)$	1.03 s
*Alpha particle power to electrons, $P_{\alpha e}$	210.7 kW
*Alpha particle power to ions, $P_{\alpha i}$	24.6 kW

* Parameters from TRANSP simulation, including those based on the Monte Carlo alpha particle model.

charges in which both deuterium NBI and combined deuterium and tritium NBI were used. The measured plasma parameters of the highest fusion performance DT discharge are shown in Table I, together with some selected parameters derived from the TRANSP code simulation[1]. In the DT cases, two discharges (pulse Nos 26 147 and 26 148) were made with 100% tritium feed to two neutral beam injectors with 78 keV acceleration, delivering 1.5 MW out of a total of 14.3 MW. In addition, a number of discharges were made with an admixture of 1% tritium in deuterium fed to two neutral beam injectors. In general, it was possible to distinguish two separate phases of each discharge: first, a good confinement H mode phase associated with rising total neutron flux and large stored energy content [12] and, second, a subsequent termination phase [13] in which the total neutron flux declined, as did the stored energy. The transition between these two phases was characterized by one of the following: an 'X event', defined as the time at which the total bolometric radiated power showed a spike of order 10–30 MW, with a simultaneous increase of the X point target temperature of the order of 100°C; a 'bloom', defined as the rollover of the deuterium density due to impurity dilution; or loss of confinement defined as the rollover of the total stored energy of the discharge. Ion cyclotron emission measurements were made throughout the PTE series of discharges.

To monitor the ICE, a two element fast wave ICRH antenna was used in reception mode as a probe (Fig. 1). The two elements of the antenna could be phased to produce either a monopole or a toroidal dipole $k_\parallel$ wavenumber spectrum (parallel to the magnetic field). In the monopole configuration, the maximum in the antenna response is centred on $k_\parallel = 0$, with a spread of $k_\parallel = \pm 4$ m^{-1}; in the dipole configuration, the reception pattern peaked at $k_\parallel = \pm 7$ m^{-1}, with a null at $k_\parallel = 0$. At typical ICE frequencies, the maximum value of $k_\parallel$ for which a fast magnetosonic wave can propagate is approximately 40 m^{-1} in the JET PTE plasma. In principle, the JET antenna could detect such waves, although with diminished sensitivity. Each antenna element was connected directly to the measurement system via two transmission lines (length $L \sim 80$ m, impedance $Z_0 = 30\ \Omega$), which have negligible loss. The power coupled to a matched load is given by

$$P_{ICE} = P_{plasma}(1 - |\rho_c|^2) \quad (5)$$

where P_{plasma} is the RF power incident on the antenna surface, the voltage reflection coefficient is

$$\rho_c = \frac{Z_0 - R_c}{Z_0 + R_c} \quad (6)$$

and the coupling resistance of the antenna is R_c. For the JET antenna system, $Z_0 \gg R_c$, and $P_{ICE} \cong (4R_c/Z_0)P_{plasma}$, showing the detected RF power to be proportional to R_c. Typical values of R_c are about 5 Ω and 2.5 Ω for the monopole and dipole cases, respectively. At the termination of the transmission lines, two transformers — one for each line — were used to match the line impedance to the 50 Ω analyser

[1] In the TRANSP simulation results quoted in this paper, the radial profile of the average effective ionic charge of the plasma, Z_{eff}, was taken from active charge exchange recombination spectroscopy measurements. In the TRANSP simulation quoted in Ref. [9] the Z_{eff} profile was assumed to be flat, with a fixed value given by visible bremsstrahlung measurements. The present procedure results in a minor difference in the estimated central thermal ion density quoted in Table I.

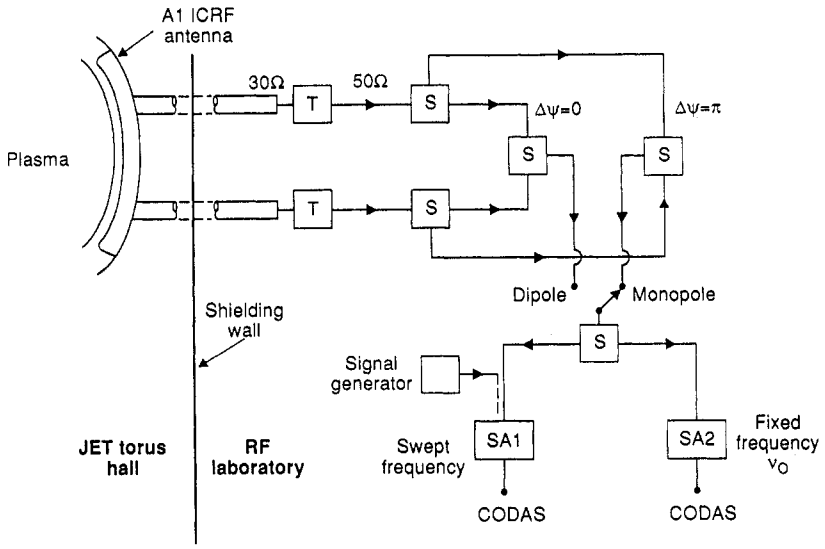

FIG. 1. Experimental arrangement used to make ICE measurements on JET tritium experiment discharges. The circuit elements marked 'T' are impedance matching transformers; those marked 'S' are power splitters. CODAS refers to the JET data acquisition system.

impedance. After combining the incoming signals with the appropriate phase, the RF signal was split equally between two spectrum analysers. These were used to monitor the ICE spectrum in a range of typically $0 \leq \nu \leq 100$ MHz or $0 \leq \nu \leq 200$ MHz by cyclically sweeping the analyser (SA1), and to monitor the time behaviour of the ICE at fixed frequency (SA2). In the swept mode of operation, the ICE spectra were sampled every 300 ms and the RF frequency was swept at a rate of 1 GHz per second. In the SA1 path, the incoming signal was mixed with calibration lines at 25 and 50 MHz, providing a reference that was stored with the data. This procedure enabled us to cross-compare data from different discharges with minimal error. The bandwidth of each analyser was 1 MHz in these experiments. For $\nu > 180$ MHz, the impedance matching transformers introduced a severe attenuation in the frequency response, effectively defining an upper limit on the bandpass. The spectra presented here have been corrected for the measured transformer response below this frequency, and have been truncated above it where the correction was so large as to be untrustworthy. No correction has been applied for the frequency response of the antenna–plasma coupling. Small impedance mismatches at the terminations of the transmission lines led to the transfer function of the system being modulated by a pattern of modes with spacing $\Delta\nu_{mode} \cong c_L/2L \sim 1.8$ MHz, where c_L is the velocity of light in the transmission line. In the spectra presented below, this structure was removed by smoothing the data with a 1.8 MHz filter, in effect limiting the resolution of the ICE measurements.

3. EXPERIMENTAL RESULTS

3.1. The power spectrum

Two ICE spectra are shown in Fig. 2, each taken just before the peak of the neutron emission in similar PTE discharges. Pulse No. 26 140 was run with pure deuterium NBI and pulse No. 26 148 with mixed deuterium and tritium NBI. Although differing in relative signal intensity, both spectra are similar in form, showing up to seven clearly identifiable and regularly spaced emission lines with narrow relative widths $\Delta\nu/\nu \approx 0.09 \ll a/R = 0.38$. In both cases, the spacing of the line centres is 17 ± 0.5 MHz. A plot of the deuterium cyclotron frequency $f_{cD}(R)$ (calculated in the total magnetic field) against major radius, R, is shown in Fig. 3. The plot shows that the spacing of the ICE line centres matches the cyclotron frequency of deuterons or alpha particles at one value of the major radius, $R = 4.0 \pm 0.1$ m. The radius of the Faraday screen of the ICRH antenna was at $R_{ant} = 4.15$ m,

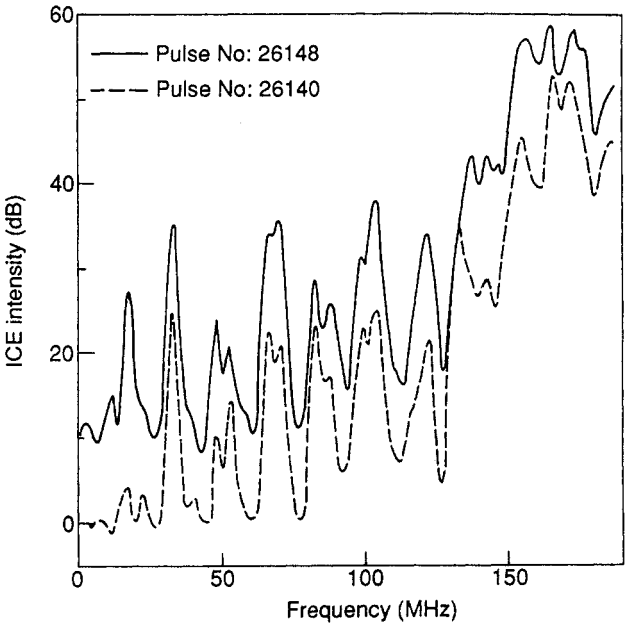

FIG. 2. ICE spectra measured in mixed DT and pure deuterium discharges. DT: solid curve, pulse No. 26 148; pure deuterium: dashed surve, pulse No. 26 140. In both cases, a monopole antenna was used and the data were taken close to the time of the peak neutron emission. The noise floor was at 0 dB for pulse No. 26 140 and at +10 dB for pulse No. 26 148.

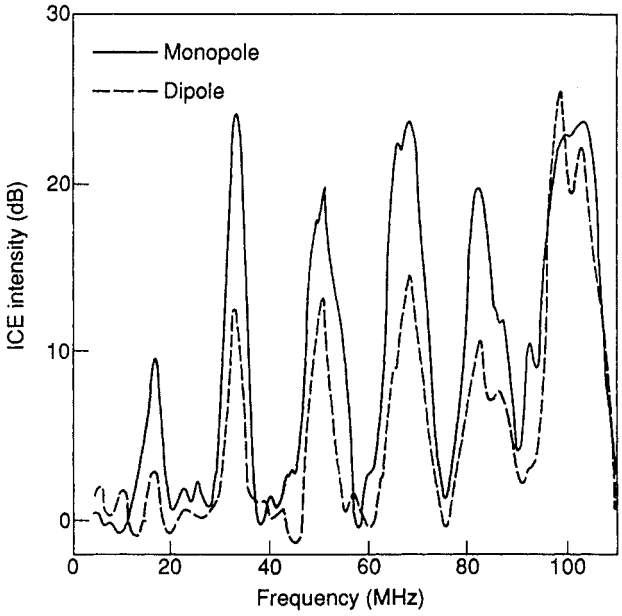

FIG. 4. Comparison of ICE spectra measured in similar NBI discharges with 1% tritium for monopole (solid curve, pulse No. 26 095) and dipole (dashed curve, pulse No. 26 108) antenna configurations.

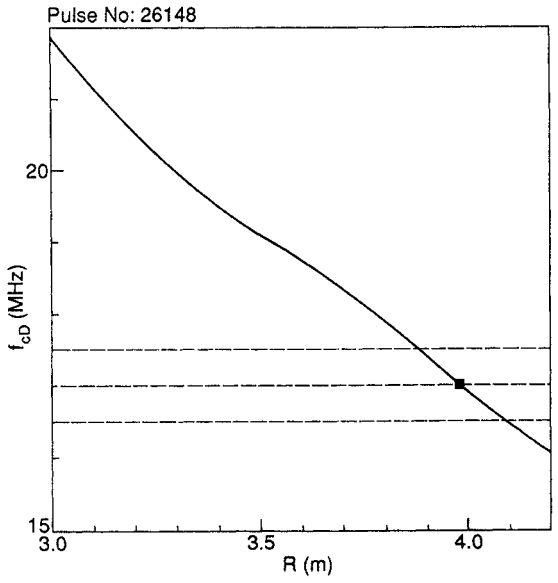

FIG. 3. The cyclotron frequency of deuterons (degenerate with alpha particles) in the total magnetic field as a function of major radius for DT pulse No. 26 148. The central horizontal dashed line represents the frequency spacing between the centres of the ICE spectral lines; the intercept shows the radius with matching cyclotron frequency. The upper and lower dashed lines represent the error limits in the measurement of the frequency spacing of the lines.

thus the emission is localized to a region close to the JET antenna. For the lower harmonics ($l \leq 7$) in the spectra of Fig. 2, the even-l lines are more intense, by up to a factor of ten. However, this feature does not appear to be a general rule, since inspection of other discharges reveals a greater degree of variability in the relative amplitudes of the sequence of lines.

A comparison between ICE spectra obtained using both the dipole and monopole antenna phasings is shown in Fig. 4, for two similar discharges with 1% tritium NBI (monopole case, pulse No. 26 095; dipole case, pulse No. 26 108). To reduce the effect of data variability, and to help reveal any clear systematic changes in the spectra, two successive spectral sweeps in each discharge were averaged together during the period of significant neutron emission. For the dipole, the lower-l lines tend to be of lower amplitude, by between 5–10 dB, compared with the monopole case. The $l = 6$ lines are, however, comparable in amplitude. Earlier work [2] has shown that the intensity of an ICE line increases linearly with the total neutron flux. Part of the amplitude difference seen in Fig. 4 can be accounted for by the fact that the total neutron flux was a factor of 2.2 larger in the discharge with the monopole phase. To reveal any underlying systematic differences in the ICE power detected

between the two cases, the spectra of a number of similar discharges were averaged in a frequency range $10 \leq \nu \leq 80$ MHz, containing the first four bright harmonic lines. It was found that the monopole dataset contained spectra that were on average twice as intense as those in the dipole dataset. This factor is consistent with the expected factor of increase in the antenna coupling resistance — and therefore in ICE power coupled to the spectrum analyser given by Eq. (5) — on changing from the dipole to the monopole configuration. We conclude therefore that, once allowance is made for the coupling resistance of the antenna, there is no significant evidence that the total ICE power that is detected is sensitive to the phasing of the JET antenna. This result shows that the power spectrum contains components with wave vectors in the acceptance range of the antenna: $0 \leq |k_\parallel| \lesssim 7\ \mathrm{m}^{-1}$.

Spectral lines from both pure deuterium and mixed DT discharges show evidence of fine structure, which can be seen in Figs 2 and 4. With increasing harmonic number, the lines appear to split into blended doublet or triplet shapes, with a linewidth given approximately by the relation $\Delta\nu/\nu \sim 0.06$. For the higher harmonics, the full width of the split lines becomes comparable with the interharmonic spacing (17 MHz). Above a frequency $\nu \sim 100$ MHz, the lines blend together into an intense continuum feature. The total power in the spectrum, integrated over the frequency range displayed in Fig. 2 is, in fact, dominated by the continuum component. The sum of the individual emission powers of the first seven clearly visible ICE harmonics represents a fraction of only about 2% of the total integrated emission power in the spectrum.

3.2. Correlation between the ICE intensity and the neutron flux

In plasmas heated with intense neutral beams, the question whether beam particles or fusion products drive the ICE was answered by comparing the level of ICE power at the $l = 2$ harmonic peak between two similar PTE discharges with pure D → D NBI (pulse No. 26 094 as the control experiment), and with mixed D + T → D NBI (pulse No. 26 148). This comparison was made at the time of peak neutron emission (Table II). The results show that, by changing from pure D to mixed D + T NBI at almost constant P_{NBI}, the ICE power increased by a factor comparable with the total neutron flux, whilst in both cases the content of beam particles in the plasma was almost constant. This shows clearly that the ICE is not driven by beam particles. In the DT case, the fusion product population of the plasma was generated predominantly by DT — and not DD — fusion reactions, showing clearly that the fusion alpha particles are responsible for the increased intensity of ICE. We add that no new lines — corresponding to triton cyclotron harmonics — were observed in discharges with tritium injection.

TABLE II. COMPARISON OF MEASURED ICE POWER WITH NEUTRON FLUX FOR TWO PTE DISCHARGES HAVING SIMILAR MAGNETIC CONFIGURATIONS AND NEUTRAL BEAM INJECTION POWERS. DISCHARGE *a* WAS RUN WITH PURE DEUTERIUM NEUTRAL BEAM INJECTION; IN DISCHARGE *b*, TRITIUM WAS INTRODUCED FROM TWO INJECTORS DELIVERING 1.44 MW AT 78 keV, AND THE REMAINING INJECTORS WERE RUN WITH PURE DEUTERIUM

Case	Pulse No. (time)	P_{NBI}	P_{ICE} (ν = 33 MHz)	Neutron flux ($\times 10^{16}$ s^{-1})
a	26 094 (13.2)	13.2 MW	0.12 μW	2.7
b	26 147 (13.2)	14.4 MW	3.1 μW	53
b/a		1.09	26	20

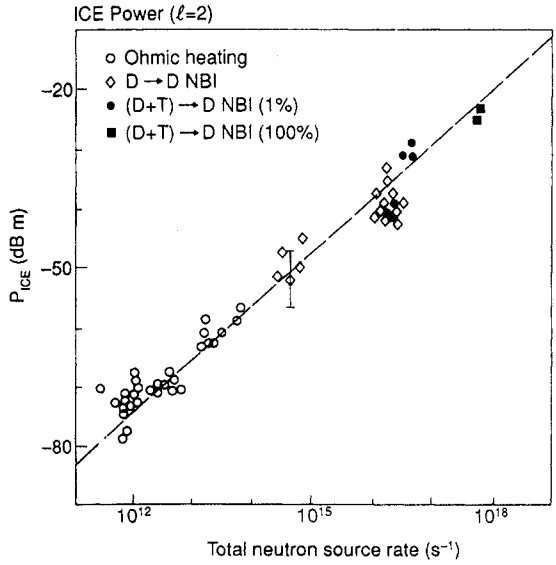

FIG. 5. Correlation between ICE intensity P_{ICE} and total neutron emission rate R_{NT} for Ohmic and NBI heated JET discharges, over six decades of signal intensity. The best fitting relation is $P_{ICE} \propto R_{NT}^{0.9\pm0.1}$.

For a wide variety of JET discharges, with Ohmic heating in deuterium, with pure D → D NBI, and with mixed D + T → D NBI, the detected ICE power has been plotted as a function of the total neutron flux R_{NT} in Fig. 5. The groups of data shown have been drawn from a database of JET ICE experiments performed between 1985 and 1991. Each data point marks the level of the ICE emission at the peak of the $l = 2$ line, which was chosen because its frequency typically lies near the resonant frequency of the ICRH antenna, $\nu \cong 33$ MHz. Uncertainties in the relative calibration between data groups arise mainly from intershot differences in the antenna coupling resistance; these are estimated to result in uncertainties of ±6 dB in detected RF power. Figure 5 shows that the measured level of the ICE power is almost proportional to the neutron flux over a range of six orders of magnitude; the best fitting relation is $P_{ICE} \propto R_{NT}^{0.9}$. The error in the exponent is ±0.1; thus these data are consistent with a linear relationship.

In the PTE discharges, whose data points occupy the upper part of the plot (total neutron source rates $R_{NT} > 10^{16}$ s^{-1}), the neutron emission source was evolving significantly — an example of the typical time evolution is shown in Fig. 6. In contrast, for the group of Ohmic deuterium discharges whose data points occupy the lower part of the plot, the neutron fluxes had reached near steady state conditions at the times the data were taken. In the time evolving discharges, the slowing down time of the fusion products is comparable with the observed growth time of the neutron emission. It follows that, at the time these data were taken, the populations of energetic fusion products were still evolving and had not yet reached steady state levels. In comparing the ICE intensities measured in dynamically evolving discharges with those in steady state conditions, it is therefore relevant to ask what level the ICE intensity would have reached if the discharge had evolved to a steady state. Taking plasma parameters at the time of the maximum neutron emission and assuming them to remain constant thereafter, we expect that, in steady state, the concentration of energetic fusion products would have reached a level approximately twice as large as that calculated at the time of the maximum neutron emission. This level would have been attained within a few slowing down times. Assuming that the ICE intensity increases linearly with the concentration of energetic fusion products, we anticipate that the data points for the time evolving discharges in the upper part of Fig. 5 should be corrected upwards by approximately +3 dB in steady state conditions. The overall effect of this correction would be to improve the quality of the linear correlation between the ICE intensity and the neutron flux in the dataset. Table III displays the relative concentrations of fusion protons and fusion alpha particles, together with the relative ICE power and neutron flux for representative pure deuterium and DT discharges. These results confirm that the ICE intensity correlates with fusion reactivity, and also shows that it does not depend primarily on the presence of specific fusion product species.

The total ICE power radiated into 4π steradians at the time of the peak neutron emission in pulse No. 26 148 is of the order of a few watts, assuming poloidal uniformity of the emission and constant

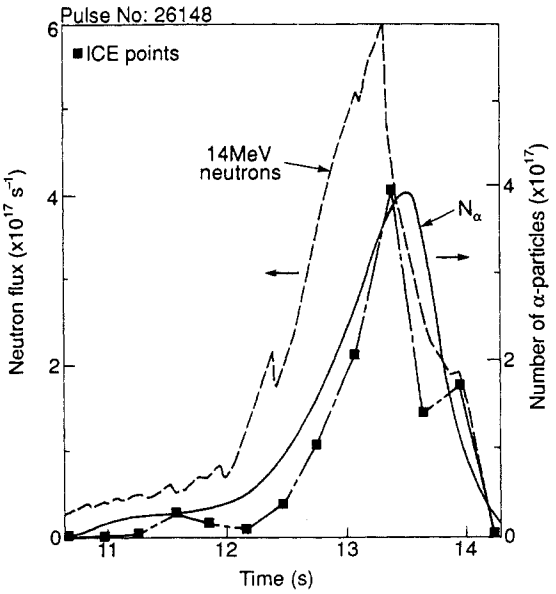

FIG. 6. Time evolution of the 14 MeV neutron emission R_{DT} (dashed line) and total number of alpha particles (solid line), compared with the integrated ICE signal (points) for DT pulse No. 26 148. The scale on the ICE power is linear.

TABLE III. DIMENSIONLESS VALUES OF FOUR PARAMETERS IN PULSE No. 26 147 (CASE *b* OF TABLE II), NORMALIZED WITH RESPECT TO THE CORRESPONDING VALUES FOR PULSE No. 26 094 (CASE *a* OF TABLE II)

	n_α	n_p	P_{ICE}	Neutron flux
b/a	~1000	0.67	26	20

coupling efficiency of the antenna in the measured frequency range. This inferred radiative power loss is a small fraction $\sim 10^{-5}$ of the total alpha particle heating power $P_\alpha \cong 235$ kW derived from TRANSP simulations (Table I) using a Monte Carlo model to describe the evolution of the alpha particle population.

3.3. Correlation between the ICE intensity and the alpha particle density

The TRANSP plasma simulation code was used both to check the internal consistency of the measured diagnostic data and to compute the spatial and temporal evolution of the energetic fusion alpha particles. The Fokker–Planck equation describing the slowing down of the energetic fusion products was solved using a Monte Carlo technique to obtain an accurate assessment of the finite orbit effects. In this model, the fast ion guiding centre trajectories, the thermalization alpha particle source, and the collisional heating rate of the background plasma are computed. During the time taken for a fusion ion to slow down to thermal energies, its confinement time is taken to be infinite — an assumption equivalent to neglecting any non-classical losses. The prompt losses of fusion ions that are born onto orbits intersecting the walls of the vessel or limiter surfaces are, however, taken into account and these particles are tracked no further. Once the energy of a confined fusion ion falls below $\frac{3}{2} T_i$, the particle confinement time is taken to be zero and the particle is no longer tracked. The birth source of fusion ions was assumed to be isotropic and monoenergetic in the reference frame of the plasma. Although this is a good assumption in the case of alpha particles produced purely by thermal DT reactions, it does not represent the birth distribution for the alpha particles produced by thermal beam DT reactions with full accuracy. Applying kinematic considerations to the two body T → D reaction, we find that fusion alpha particles produced in NBI thermal beam collisions are born with a spread of energies in the laboratory frame. The range extends from $E_\alpha = 3.6$ MeV − 0.7 MeV = 2.9 MeV (in the direction opposite to the motion of the beam ion) to $E_\alpha = 3.6$ MeV + 0.8 MeV = 4.4 MeV (in the forward direction with respect to the motion of the beam ion) for the tritium beam injection energy of 78 keV used in the experiments. Approximately half the alpha particles were produced by thermal beam DT reactions in the two pulses, Nos 26 147 and 26 148. We therefore expect some angular and energy spreads in the experimental alpha particle birth distribution. The fast ion radial density profiles were computed as flux surface averages, and the alpha particle density profile for DT pulse No. 26 148 is shown in Fig. 7. The effect of including the finite Larmor radii of the fast ions is to broaden the density profile, an effect that is particularly significant in the edge region where the radial gradient is steep. This effect was estimated by convolving the TRANSP alpha particle radial density profile with the alpha particle Larmor radius, and the corrected density profile is shown in Fig. 7. For trapped energetic fast ions, the orbit geometry gives rise to strong poloidal asymmetry, favouring population of the low field side of the torus with fusion ions having large velocities perpendicular to the magnetic field. Thus the flux surface averaged fusion product density shown in Fig. 7 underestimates the local number density at the outer edge of the plasma. For trapped orbits of the type shown in Fig. 14(b), the local density of fusion products at the outer midplane edge, $R = 4.0$ m, is approximately six times larger than the value calculated by flux surface averaging. Allowing for the effects of finite alpha particle Larmor radius and of poloidal asymmetry, we estimate that, at the location of the ICE source and given the conditions of Fig. 7, the local density of energetic alpha particles is

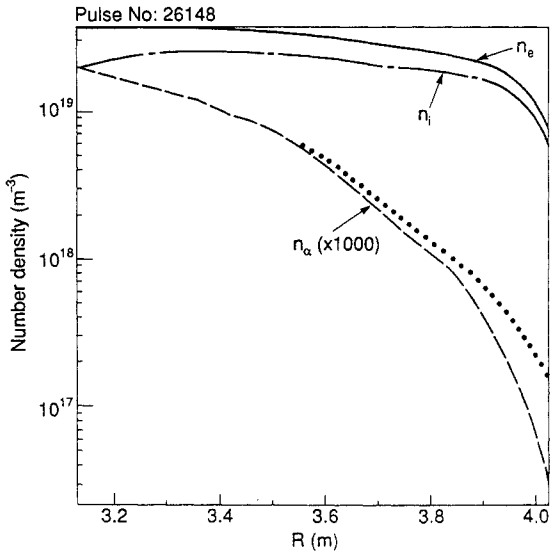

FIG. 7. Radial density profiles of ions, electrons and alpha particles in DT pulse No. 26 148 at time t = 13.2 s. The magnetic axis is at major radius R = 3.13 m. The alpha particle density was computed from the TRANSP Monte Carlo model based on guiding centre orbital trajectories, averaged over each flux surface. The dotted curve shows the effect on the alpha particle density profile of the broadening due to the finite Larmor radius of the alpha particles. The radial ion density profile refers to thermal ions only; the injected beam ion density profile is not shown.

$n_\alpha (R = 4.0\ \text{m}) \sim 10^{15}\ \text{m}^{-3}$. This is considerably smaller than the central value, $n_\alpha (R = 3.13\ \text{m}) \approx 2.0 \times 10^{16}\ \text{m}^{-3}$.

Traces from the fixed frequency spectrum analyser show large ($\sim 100\%$) fluctuations in the ICE amplitude at the data sampling frequency (2 kHz). The bursts appear to be coherent within the emission volume, since, if this were not the case, and the emission volume was to contain multiple, uncorrelated bursting regions, the resulting depth of modulation would be less than 100%. In order to compare the fluctuating ICE signal with the calculated alpha particle densities, individual spectra were therefore averaged in the available range of the swept analyser, 10–180 MHz, to yield a signal representing the average ICE power. A comparison of the temporal evolution of the integrated ICE signal with the measured total 14 MeV neutron flux is shown in Fig. 6. Up to the time of the X event ($t = 13.28$ s), the integrated ICE signal follows the neutron emission, but is delayed by a time of approximately 0.5 s. We found a delay of similar magnitude in D → D NBI discharges, and the effect has also been observed in D → D NBI discharges on TFTR [7]. The delay of the ICE signal with respect to the rise of the neutron flux is comparable with the time needed to build up a population of fusion products, namely the fusion ion–electron slowing down time τ_s. During the rise phase of the 14 MeV neutron emission, between 12 and 13.28 s in DT pulse No. 26 148 (Fig. 6), the volume averaged value of τ_s is in the range 0.6–0.7 s, a value consistent with the observed delay. A comparison of the temporal evolution of the integrated ICE signal with the total number of energetic alpha particles N_α — as given by the Monte Carlo calculation — is shown in Fig. 6. The ICE data point with the largest signal intensity has been normalized to the peak number of alpha particles for comparison. Up to the time of the X event, the ICE signal correlates reasonably well with the calculated total number of alpha particles. However, between 12.5 and 13.3 s, the ICE intensity increases more rapidly than N_α.

As noted above, frequency matching considerations for the harmonic ICE spectral peaks imply a major radius of $R = 4.0 \pm 0.1$ m for the location of the source of emission. It is therefore appropriate to compare the intensity of the ICE signal with the evolution of the number density of alpha particles at the plasma edge. As we shall discuss in Section 4.2, the fusion product population in the outer edge plasma is dominated by energetic particles that are born in the core, but whose drift orbits undergo large radial excursions. Figure 8 shows a comparison of the time evolution of the ICE data and of the number density of alpha particles at three major radii from the centre to the edge of the plasma: $R = 3.13$, 3.38 and 4.0 m. The peak of each curve has been normalized to the largest ICE data point. The sudden drops in the two innermost alpha particle density traces are the result of the sawtooth model used in the TRANSP simulation. In this, the sawtooth is assumed to redistribute all the fast ions inside the $q = 1$ surface (normalized radius $r/a \sim 0.36$) uniformly in a mixing region of normalized radius $r/a \sim 0.51$. Up to the time of the first sawtooth, the ICE data lie significantly below the two innermost alpha particle density traces. At the time of the sawteeth, there is clearly no significant response in the ICE signal, a feature shared by the edge alpha particle density trace. Up to the time of the X event, however, the ICE data and the edge alpha particle density trace are closely correlated. The best fit between the measured ICE data points and the curves of evolving alpha particle density occurs for major radii between $R = 3.93$ m and $R = 4.0$ m, a feature consistent with the results of frequency matching to the ICE spectral lines (Fig. 2).

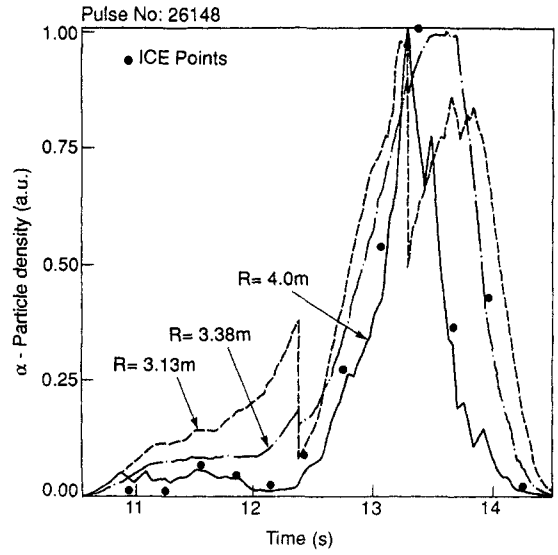

FIG. 8. Time evolution of the alpha particle density at selected radii, compared with the integrated ICE signal (points) for DT pulse No. 26 148.

After the time of the X event, during the termination phase, the discharge shows a period of intense edge MHD activity with the appearance of large amplitude ELMs. This phase also coincides with observations of enhanced, broadband fluctuations in edge density revealed by the microwave reflectometer diagnostic. As discussed below, in Section 3.4.2, this MHD activity strongly affects the ICE measurements.

Thus, after the X event time (t = 13.28 s) in this discharge, it should be noted that the spectrally integrated ICE data shown in Figs 7 and 8 are distorted by these effects.

3.4. Correlation of the ICE with MHD observations

3.4.1. Central MHD activity (m = 1, n = 1)

Earlier ICE observations in JET high current (I_p = 6 MA) ohmically heated discharges [6] showed clear evidence of a positive correlation between ICE fluctuations and sawtooth collapses. The ICE signal increased approximately 20 ms after the central sawtooth collapse, a delay comparable with the measured propagation time of the heat pulse to the edge. Figure 9 shows the time variation of the fixed frequency (ν = 33 MHz) ICE signal during the good confinement phase of DT pulse No. 26 147. The times of three sawtooth collapses are marked. Following each sawtooth collapse, there is a small fluctuation in the ICE signal. Inspection of other discharges in the PTE series revealed some further correlations with inverted sawteeth, although in these lower current (I_p = 3.1 MA) discharges the correlation is not as clear as that observed in the higher current discharges [6]. In some cases, sawtooth collapse produces no observable change in the ICE signal. In addition, we have found no convincing evidence for correlation of the ICE fluctuations with fishbone bursts. Therefore, in the PTE discharges, there is no consistent evidence for a correlation between ICE fluctuations and central m = 1, n = 1 activity.

3.4.2. Edge localized MHD modes (ELMs)

A variety of ELM phenomena has been observed in JET H mode discharges. For comparison with the ICE signal, we divide the ELMs into two classes: large and small amplitude ELMs. Soft X ray measurements show that the small ELMs perturb only the outermost few centimetres of plasma, whereas the large ELMs penetrate to depths of between 10 and 30 cm. Radically different behaviour in the ICE signal is observed in the two cases.

Small amplitude ELMs are commonly observed, for example, in the L to H transition and during the early part of the good confinement phase of the high performance PTE discharges. Examples of these are shown by the D_α spikes in Fig. 9. Time resolved data show a number of discrete ICE amplitude fluctuations of approximate duration 20 ms, and amplitude $\Delta P_{ICE}/P_{ICE} \sim 1$

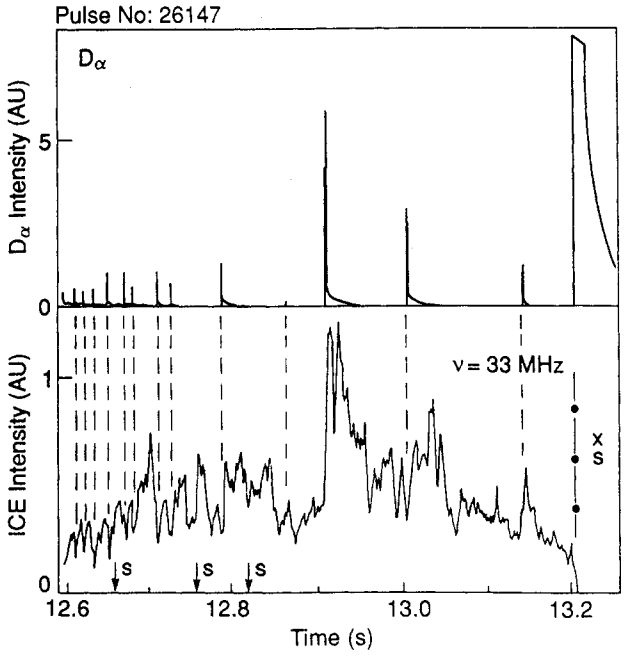

FIG. 9. Comparison of the ICE signal with ELM events showing correlation prior to the X event, for DT pulse No. 26 147. The times of sawtooth collapse are denoted by the symbols 'S', and the X event and associated sawtooth collapse by 'XS'.

which, in general, correlate positively with these ELMs. As noted in Section 2, the detected ICE signal is proportional to the product of the ICE source power in the plasma with the antenna-plasma coupling resistance R_c, which is always observed to increase when ELMs occur. During ICRH heating experiments in the presence of ELMs, fluctuations of magnitude $\Delta R_c/R_c \sim 1$ are commonly observed. Thus, during the good confinement phase of the discharge, the positive correlation observed between ICE and small amplitude ELMs is consistent with ELM induced changes in R_c, and not with any change in the intrinsic strength of the ICE source. Corresponding soft X ray data reveal only small amplitude perturbations in the outermost few centimetres of the plasma. We infer that these small amplitude ELMs do not penetrate sufficiently far into the edge plasma to disturb the ICE source.

However, during the termination phase of PTE discharges, ELMs of significantly larger amplitude are observed. Examples of large amplitude ELMs coinciding with the X events in DT discharges are shown in Figs 9 and 10. Coincident with the appearance of a large ELM, the ICE signal vanishes in a time less than 500 μs. We conclude from this that the large amplitude ELM is associated with the prompt loss of alpha particles from the edge. In both pure deuterium and mixed

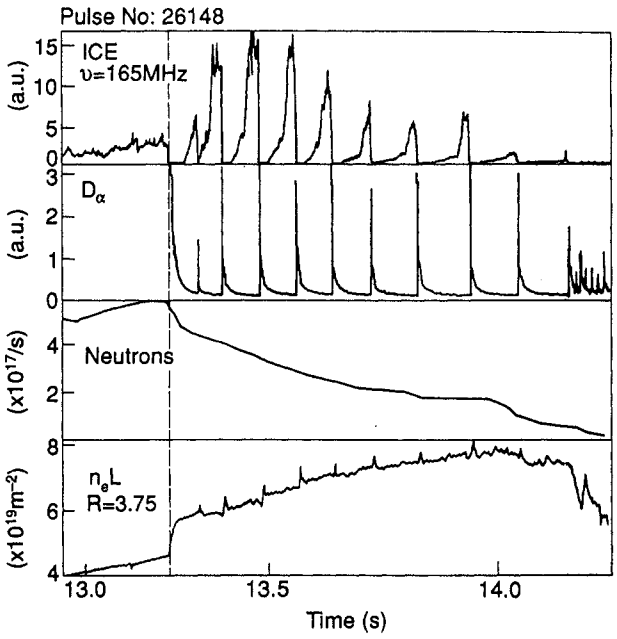

FIG. 10. The termination phase of DT pulse No. 26 148, showing the correlation with ELMs of the ICE, a D_α signal, the total DT reaction rate R_{DT}, and the electron density integrated along a line of sight tangent to the flux surfaces at R = 3.75 m. The X event occurred at time t = 13.28 s, shown by the vertical dashed line.

DT discharges, the ICE vanishes at the time of each large amplitude ELM. An example of this behaviour is shown in Fig. 10 for DT pulse No. 26 148, in which a sequence of large amplitude ELMs, having repetition times in the range of 60–100 ms, was observed after the X event. For this discharge, the fixed frequency spectrum analyser was tuned to a frequency of 165 MHz, close to the tenth harmonic of the edge alpha particle cyclotron frequency and lying in the continuum part of the spectrum. Inspection of the corresponding ICE spectra revealed, in addition, that lines with harmonic numbers l = 3–9 were completely absent for a period of approximately 20 ms following each ELM. No coincidence data were available for the l = 1 and 2 harmonic lines in this discharge. It appears that the whole of the ICE signal, including both continuum and edge ICE peaks, vanishes at the time of a large amplitude ELM. Simultaneous soft X ray data show large perturbations penetrating to a depth of between 10 and 30 cm in the edge plasma, which encompasses the ICE source. There are coincident peaks in the visible D_α line radiation. We infer that the large amplitude ELMs terminate the ICE by expelling fast ions, thereby temporarily extinguishing the source. This behaviour is consistent with the localization of the ICE source in the edge, and also shows that there is little or no contribution to the ICE signal from the fusion products that are confined to the discharge core. Figure 10 also shows the behaviour of the line integrated electron density in an outer channel of the millimetre wave multichannel interferometer, having line of sight tangential to the magnetic flux surfaces at major radius R = 3.75 m. At the time of the X event, there is a sudden upward step in the edge plasma density. Subsequently, the trace shows transient increases correlated with the ELMs. The Abel inverted density profile shows that this density step is particularly significant for major radii between $R \sim$ 3.7 m and the outer edge, and persists for the ELM phase shown in Fig. 10. An increase in the plasma density in front of the ICRF antenna increases the antenna–plasma coupling resistance, and leads to a corresponding increase in the ICE power detected. This effect may explain the increase in the peak level of detected ICE intensity seen after the time of the X event in Fig. 10.

The time expanded traces of Fig. 11 show that each successive ELM in the sequence annihilates the ICE for a period of about 20 ms before a new phase of growth occurs. During this temporary period of ICE quiescence, microwave reflectometer data show a high level of broadband edge plasma density fluctuations with frequencies up to 100 kHz [14]. These fluctuations coincide with the period when the D_α signal remains above the background level. As the D_α signal

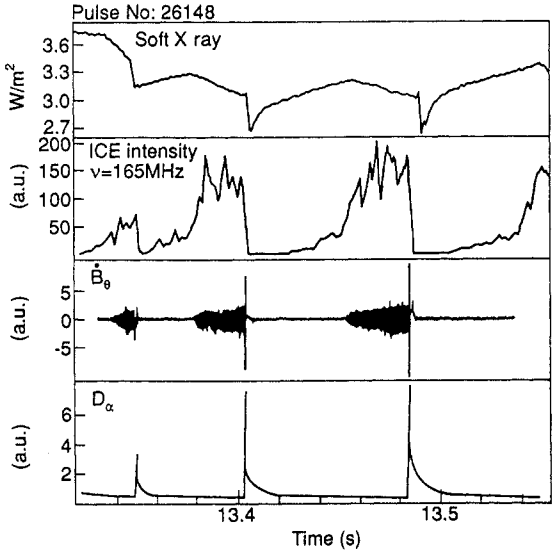

FIG. 11. Time expanded view of the termination phase of DT pulse No. 26 148, showing details of the correlation with ELMs of the ICE, a D_α signal, an MHD coil mounted at the top of the vessel, and a soft X ray line of sight at major radius R = 3.98 m.

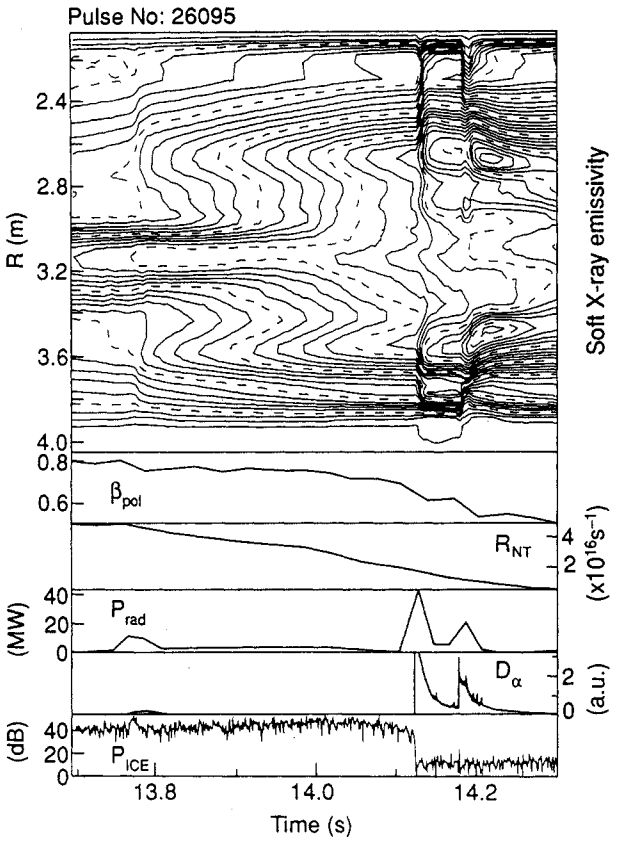

FIG. 12. Evolution of the PTE pulse No. 26 095 with 1% tritium injection in two neutral beam sources. Above: reconstructed contours of soft X ray emissivity as a function of time and major radius. Below: corresponding traces of poloidal beta β_{pol}, total neutron flux R_{NT}, total bolometric radiated power P_{rad}, a D_α signal, and the ICE intensity at fixed frequency ν = 33 MHz.

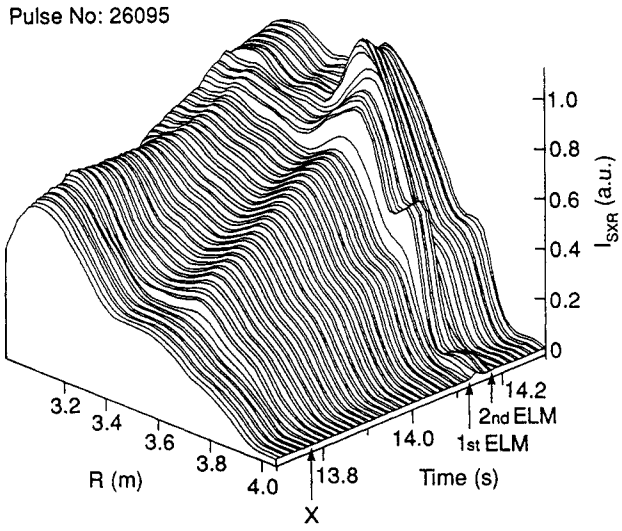

FIG. 13. Isometric projection of the time evolution of the reconstructed soft X ray emissivity radial profile for pulse No. 26 095. The time of the X event is marked by the symbol X, and the times of the two subsequent large amplitude ELMs are shown.

decays, a new phase of ICE growth commences, consisting initially of slow growth for a time of about 15 ms, followed by rapid growth. During the phase of rapid growth, magnetic coil data show bursts of 4.5 kHz MHD oscillations. The form of the growth of these oscillations is initially exponential, but subsequently follows a linear law; this latter phase coincides with a saturation of the ICE signal. Eventually the ICE and MHD oscillations are both terminated by the next ELM. Soft X ray data (Fig. 11) show a deformation associated with the mode which is largest at the q = 2 surface (which intersects the outer major radius at $R \sim 3.8$ m), indicating an m = 2, n = 1 mode. The 4.5 kHz MHD mode has not been observed in any of the 1% tritium PTE discharges or in other similar DD discharges, and it appears to be a unique observation in the two 100% tritium PTE discharges.

X events can also occur without the prompt disappearance of the ICE signal, as shown in Fig. 12. In pulse No. 26 095, the X event occurs at t = 13.78 s. Tomographic reconstruction of the soft X ray emission prior to the X event shows a peaked profile, characteristic of a phase of good confinement. However, at t = 13.78 s, the total neutron flux starts to fall and there is a modest drop in central β coincident with a radiation spike of amplitude $P_{rad} \sim$ 15 MW. The ICE signal shows a transient increase lasting about 20 ms, but, unlike the case of pulse No. 26 148, survives the X event. At this time, the soft X ray emission contours show a relatively slow flattening of the profile, and there is only a mild deformation in the edge region at $R > 3.7$ m, a feature that can also be seen in Fig. 13. However, at time t = 14.13 s, a faster event occurs, which affects a large region of the profile causing a significant drop in central β and a larger radiation spike of amplitude $P_{rad} \sim$ 42 MW. At this time the ICE signal disappears and does not recover subsequently. The large D_α spike is characteristic of a large amplitude ELM, and the reconstructed soft X ray emission contours show a deformation extending a radial distance of about 50 cm into the plasma from the edge. A second, large amplitude, ELM occurs shortly afterwards at t = 14.18 s. Similar behaviour was also observed in the pure deuterium pulse No. 26 094. These observations show that a necessary condition for the sudden disappearance of the ICE signal is the occurrence of an ELM of sufficiently large amplitude to perturb the edge plasma significantly in the region of the ICE source. This does not necessarily have to coincide with loss of the central confinement, nor with the rollover of the neutron emission due to impurity dilution.

4. GENERAL PROPERTIES OF THE EMISSION

4.1. Experimental constraints on theoretical models of ICE

In seeking a plausible ICE mechanism, the range of possible theoretical models is strongly constrained by a number of experimental considerations. First of all, the evidence from JET discharges with Ohmic heating in deuterium, with pure D → D NBI, and with mixed D + T → D NBI shows that charged fusion products provide the free energy to drive the ICE. The intensity of an ICE peak is observed to increase almost linearly with the neutron flux — and therefore approximately with the number of energetic fusion products in the discharge — over a range of six decades in signal intensity. However, pure deuterium and mixed DT discharges contain different primary fusion products. The candidate primary pure deuterium fusion products from reactions (1) and (2) in pure deuterium are 3 MeV protons, 1 MeV tritons and 0.82 MeV ^{3}He nuclei; in the 100% PTE DT case, the dominant fusion product is the 3.6 MeV alpha particle produced in reaction (4). In the DT experiments, a diffuse background of pure deuterium fusion products is also present, just as in the pure deuterium cases there is a diffuse population of energetic alpha particles arising from the burnup of the primary tritium and ^{3}He products in secondary fusion reactions. The secondary products are, however, produced at a rate significantly lower than that of the primary products. For example, tritons are born with energies well above the maximum cross-section for DT reactions and the typical fraction of tritium burnup in the present pure deuterium experiments is of the order of 1%. It is remarkable that the ICE power spectra in the pure deuterium and mixed DT experiments are so similar in form — although different in relative intensity — given the different reaction rates and concentrations of fusion products of differing species.

A further important constraint on theoretical models arises from the observed spatial localization of the emission at the outer midplane edge of the JET plasma, for which there are three independent pieces of evidence. First, the observed frequencies of the spectral lines match the successive deuteron or alpha particle cyclotron harmonics at the edge. Second, there are time resolved observations [6] of ICE sawtooth oscillations, which are inverted and show a short time delay with respect to the central sawtooth collapse. Third, the disappearance of the ICE signal is simultaneous with large amplitude ELMs, which penetrate 10–30 cm into the edge plasma. In addition, the dynamical evolution of the ICE signal is more consistent with the rate of rise of alpha particle density at the edge than at the centre. The band of major radii implied by these observations is $3.9 \leq R \leq 4.1$ m. This narrow band of radii could hardly be smaller in view of the fact that energetic fusion products are responsible for the emission, since the Larmor radii of 3.6 MeV alpha particles and of 3 MeV fusion protons can be as large as $\rho_\alpha \sim 12$ cm in the outer edge of the PTE discharge. This implies that the energetic particles responsible for the ICE almost graze the limiter. If their orbital guiding centres were to be displaced outwards by a distance small compared with the gyroradius, they would strike the limiter surface and be promptly lost from the plasma. Frequency matching considerations cannot be used to analyse the broad continuum radiation which is dominant above a frequency of about 100 MHz in both pure deuterium and mixed DT JET discharges. The ICE continuum is, however, clearly also sensitive to the presence of energetic fusion alpha particles in the plasma, as can be seen in Fig. 2. With the injection of tritium into the plasma, the ICE power at frequencies above 100 MHz increases relative to the pure deuterium case by a factor of typically 10–30, similar to that observed in the lower harmonic peaks. It is possible that the continuum arises from the overlapping and blending together of the high l number emission lines, although we cannot rule out a secondary continuum emission mechanism on the basis of the present experimental results.

The range of possible emission mechanisms is further constrained by the absolute intensity of the ICE. We can compare the measured absolute ICE signal level with the underlying thermal black body power emitted by two ion populations in the plasma, namely thermal deuterons with average temperature $T_D = 10$ keV, and a population of fusion alpha particles having a classical slowing down distribution and effective temperature $T_\alpha = 1.3$ MeV. If an antenna is placed inside a black body enclosure at a temperature T, the black body power coupled is $P_{BB} = \frac{1}{2} k_B T$ Hz^{-1}, where k_B is the Boltzmann constant, and the factor of 1/2 comes from the fact that any antenna receives only one polarization. From the thermal deuterons we expect $P_{BB} = -70$ dB·m, and from the alpha particles, $P_{BB} = -50$ dB·m. These figures would relate to an optically thick plasma. Comparing these levels with the data shown in Fig. 5, we see that the most intense ICE signals from the DT discharges exceed the highest value of P_{BB} by a factor of approximately 500, confirming the highly superthermal nature of the ICE. In fact, self-absorption is expected to be small in the

present DT discharges, which have central alpha particle number density $n_\alpha \sim 10^{16}$ m^{-3}, so that the full black body level would not be attained.

In our search for a plausible explanation for the measured ICE signals, the above considerations exclude models based on cyclotron radiation from ensembles of charged particles gyrating in the magnetic field. First, even if the plasma were optically thick in this frequency range, we have seen that the observed radiation intensity exceeds the black body level by a factor of at least 500. Second, such models would predict radiation from the whole population of energetic ions. Since these are concentrated in the plasma core, they would emit cyclotron radiation in harmonic lines substantially broader and at higher frequencies than those observed. A two dimensional, full wave ICRF code has been used to model the ICE spectrum that would arise if it were appropriate to use the statistics of the local fluctuating current spectrum [15]. These calculations were based on radiation from a slowing down distribution of energetic fusion products in the plasma core. For simulated JET conditions with a population of fusion alpha particles, individual cyclotron harmonic structure is not present for harmonic numbers $l \geq 2$. This is because, at these high frequencies, more than one harmonic is present in the plasma, causing harmonic overlap and giving rise to a broad spectrum. It is clear that these predictions are inconsistent with the narrow ICE spectral lines observed. Presumably the ion populations do emit thermal cyclotron radiation, but this must be at an intensity lower than is observed in the experiments. We conclude that a more efficient line radiation mechanism must occur at the plasma edge, one that effectively masks the underlying thermal radiation.

We next investigate the detailed structure, in velocity space, of the distribution of the energetic fusion products, paying particular attention to the critical region in the outer edge plasma.

4.2. The distribution of fusion products at the plasma edge

The experimental evidence from both Ohmic and NBI heated discharges shows that the superthermal ion cyclotron line emission originates from fusion products in the outer edge of the plasma. However, the source of DD and DT fusion products has a centrally peaked radial profile, which raises the question of how the ICE can be localized in a region where fusion birth is negligible. This problem can be resolved by considering the properties of the drift orbits of the energetic particles. Calculations show the existence of a special class of fusion products, born onto trapped orbits within a narrow range of pitch angles in the core plasma, whose drift orbits intersect the outer midplane edge, defined in JET as the band of major radii $3.9 \leq R \leq 4.1$ m. For future convenience, let us designate the class of fusion products, which are born in the core plasma and whose drift orbits reach the plasma edge, as large excursion (LE) particles. We have used a single particle full orbit code [16] to show that this special class of energetic fusion products occupies a narrow range of trapped pitch angles, just inside the trapped-passing boundary. To illustrate this, in Fig. 14 we show alpha particles launched in the magnetic geometry of DT pulse No. 26 148 with initial birth position $R_{\text{birth}} = 3.46$ m, $\theta_{\text{birth}} = 0$. This birth position lies in a region of significant alpha particle production. The magnetic axis is at $R_0 = 3.13$ m and the last closed flux surface at $R = 4$ m. Figure 14(a) shows the passing orbit of an alpha particle with a pitch angle of 54.8°, just below the trapped-passing boundary. However, a small increase in the birth pitch angle to 55.2°, moves the particle into the trapped region, producing the trapped orbit shown in Fig. 14(b). For larger values of the birth pitch angle, the maximum orbital radius decreases; an example is shown in Fig. 14(c) where the pitch angle is 65.1°, giving a trapped orbit that does not quite intercept $R = 4$ m.

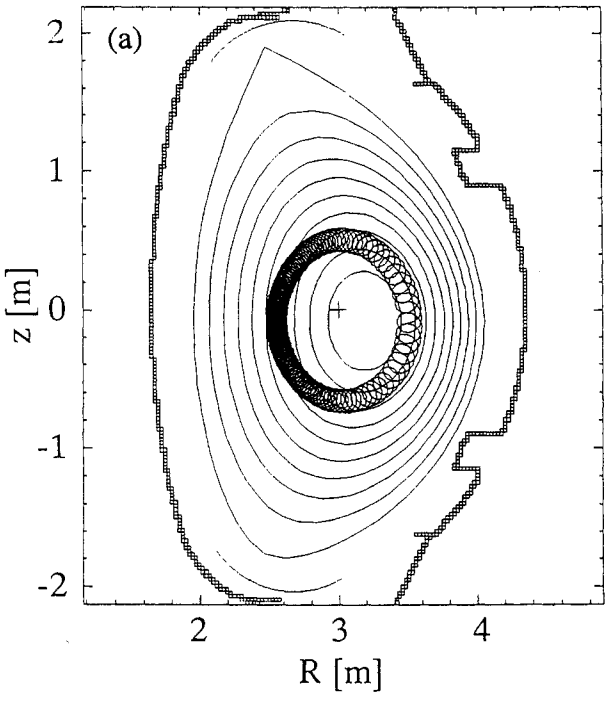

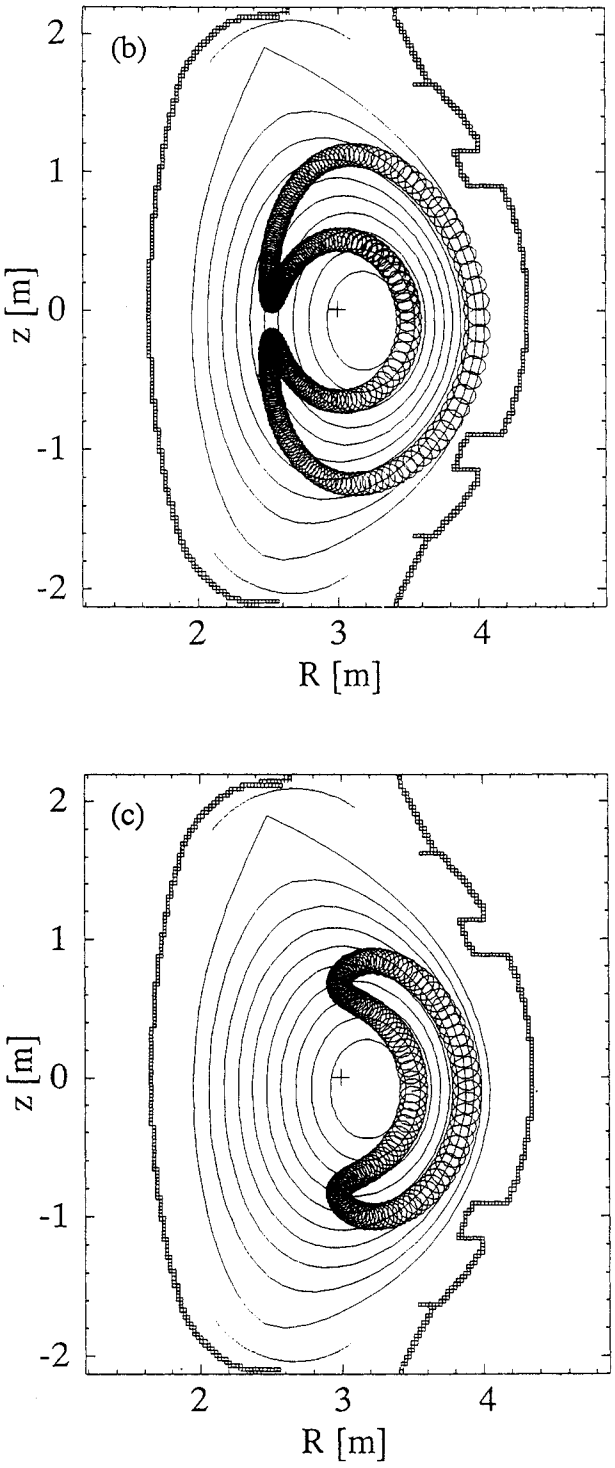

FIG. 14. Poloidal projection of 3.6 MeV alpha particle orbits in the flux surface geometry of DT pulse No. 26 148 at time 13.2 s, close to the time of maximum neutron emission (see Fig. 6). In each case the particle was born at a point 33 cm from the magnetic axis in the midplane. (a) A passing orbit, just below the trapped-passing boundary — birth pitch angle 54.8°. (b) A large excursion (LE) trapped orbit, just above the trapped-passing boundary — birth pitch angle 55.2°. (c) A trapped orbit that does not quite intercept R = 4 *m — birth pitch angle 65.1°.*

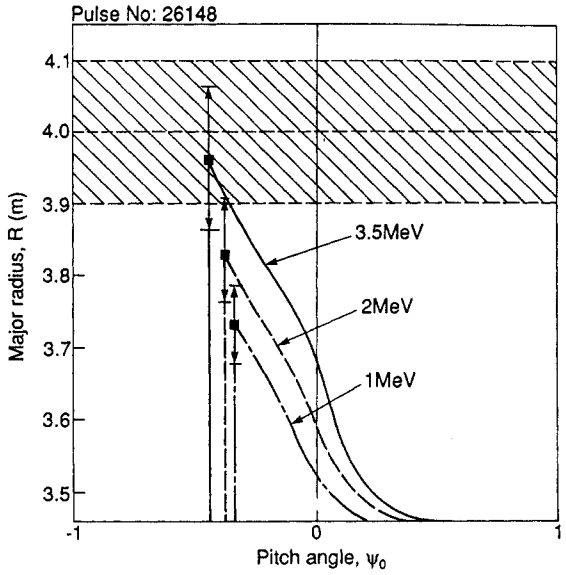

FIG. 15. Plot of the maximum radial excursions of alpha particle guiding centre orbits as a function of the birth pitch angle, for particle energies of 3.5, 2 and 1 MeV. The hatched region (3.9 ≤ R ≤ 4.1 m) represents the location of the ICE source. The vertical lines positioned at the maxima of each curve represent plus or minus one Larmor radius.

Below the lower limit on the pitch angle at 55.0°, the orbits are passing. We can estimate the fraction of alpha particles born into LE orbits, assuming an isotropic birth distribution in velocity space, as follows. Taking the values $\psi_2 = 55.0°$ and $\psi_1 = 65.1°$, which define the limits on the LE range, and noting that the solid angle lying between two pitch angles ψ_1 and ψ_2 is $d\Omega = 2\pi(\cos\psi_2 - \cos\psi_1)$, we find that a fraction $d\Omega/4\pi \approx 8\%$ of the 3.6 MeV alpha particles at this birth position are born into LE orbits. The orbits of particles born elsewhere in phase space remain close to the plasma core.

Figure 15 shows the maximum radial excursion of the alpha particle guiding centre orbits away from the birth radius, $R_{max} - R_{birth}$, as a function of pitch angle at birth, $\psi_0 = v_{\|0}/v_{\alpha 0}$, where $v_{\alpha 0}$ is the alpha particle birth velocity. At this birth position, only those alpha particles making drift radial excursions larger than 0.54 m can reach major radii $R \geq 4.0$ m. It follows that the velocity distribution of the fusion products at the outer midplane edge should be exceptionally anisotropic compared with the velocity distribution elsewhere. As the LE ions slow down, their orbits contract, so that below a certain energy they no longer intercept the edge. The maximum radial excursions of

partially thermalized (2 and 1 MeV) alpha particles is also shown in Fig. 15. Only the outermost tips of the Larmor orbits of a fraction of the 2 MeV alpha particles can reach $R = 4.0$ m, and none of the 1 MeV alpha particles can do so. Thus the region of velocity space (at $R = 4.0$ m, at the midplane) containing the orbits of alpha particles is cone shaped (Fig. 16). The cone is bounded, at the top, by the birth velocity of newly born alpha particles ($v_{\parallel}^2 + v_{\perp}^2 = v_{\alpha 0}^2$). On the left hand side is the trapped-passing boundary, and the boundary on the right is determined by the decrease in orbital radius shown in Fig. 15. The distribution of alpha particles at the edge therefore resembles a *ring* in velocity space and is accordingly maximally anisotropic and non-monotonic.

It is difficult to determine the radial extent of velocity space anisotropy using the single particle approach. Nevertheless, it is possible to treat analytically the broadening effect of the drift orbits on the radial density profile of 3.6 MeV alpha particles, in a model [17] where the safety factor is assumed to be independent of radius, and the energetic population divides into two classes: trapped and circulating particles. Applying this model to pulse No. 26 148 gives the radial profiles shown in Fig. 17. The plot shows that, at large normalized radii $r/a > 0.8$, in a region of low alpha particle production, the density is dominated by trapped ions produced near the plasma core. The excess is balanced by a modest reduction in the alpha particle density at smaller radii. This leads naturally to an anisotropic edge velocity distribution in the outer midplane of the tokamak. Figure 17 shows the anisotropy of the alpha particle distribution (ratio of trapped to untrapped alpha particle density). Up to a normalized radius of 0.8 the ratio is close to unity,

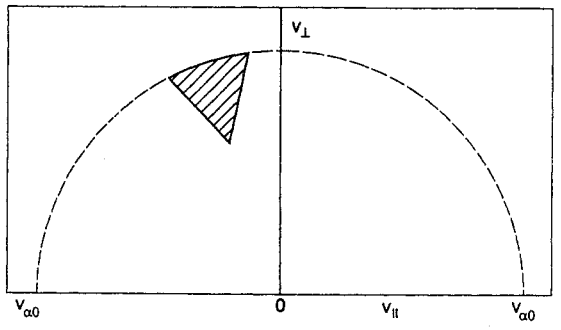

FIG. 16. The region of velocity space occupied by centrally born alpha particles with large excursion (LE) orbits at major radius R = 4.0 m. Parameters are for JET pulse No. 26 148, as in Fig. 14.

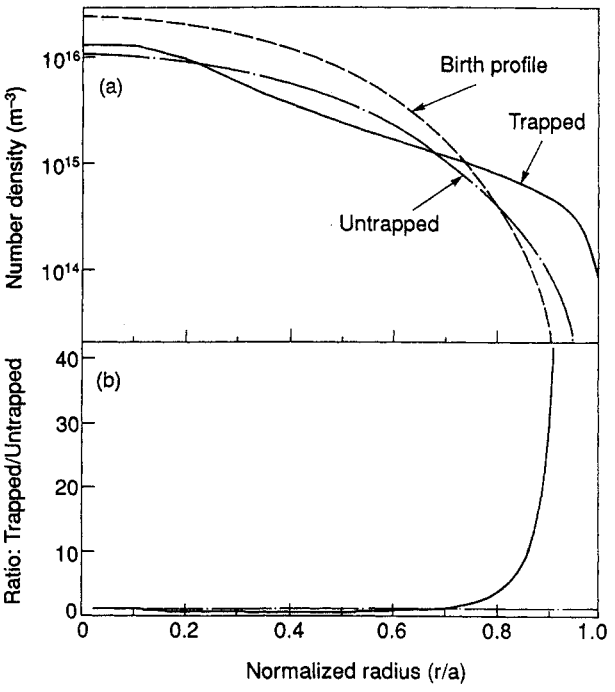

FIG. 17. (a) Profiles of the density of birth, trapped, and passing 3.6 MeV alpha particles. (b) Anisotropy ratio of trapped-passing alpha particle density. The horizontal chain line shows the isotropic case where the ratio of trapped-passing alpha particle density is unity.

indicating approximate isotropy. For $r/a > 0.8$, the anisotropy increases dramatically on the low field side of the torus where the LE orbits, such as the one shown in Fig. 14(b), enhance the local density.

5. ORIGIN OF THE ION CYCLOTRON EMISSION

5.1. Collective relaxation in the edge plasma

In view of the highly superthermal nature of the observed ICE, and its spatial localization in a region of the plasma where the fast ion velocity distribution is likely to be maximally anisotropic and non-monotonic, it is reasonable to seek an explanation for the radiation in terms of collective instability and relaxation. A source of free energy can be made available to drive instabilities from anisotropy

$$\partial f_\alpha/\partial v_\perp \neq \partial f_\alpha/\partial v_\parallel \qquad (7)$$

or non-monotonicity

$$\partial f_\alpha/\partial v_\perp > 0 \qquad (8)$$

or radial inhomogeneity

$$\partial f_\alpha / \partial r < 0 \tag{9}$$

of the fast ion velocity distribution function f_α. As we have seen above, each of these terms is likely to be a feature of the fusion product distribution in the edge plasma.

As a possible explanation of the ICE in terms of a collective instability driven by the energetic fusion products, we consider the excitation of the fast wave by ion cyclotron instability (ICI) [18–21]. The essential theoretical feature of the ICI model is the liberation of free energy from the fast ions to excite waves on the fast Alfvén-ion Bernstein branch, propagating across the magnetic field with frequencies close to the ion cyclotron harmonics.

For perpendicular propagation, resonance occurs between the fast wave and the negative energy cyclotron harmonic waves supported by the superthermal ions [18–21]. In a plasma with a dilute, superthermal ion component it is possible to excite waves on the fast Alfvén-ion Bernstein branch of the dispersion relation, propagating in the direction perpendicular to the magnetic field at harmonics of the superthermal and background ion cyclotron frequencies, Ω_α and Ω_i. The real frequency of this instability is given by

$$\omega \cong \omega_0 \equiv c_A k = l\Omega_\alpha \tag{10}$$

where c_A is the Alfvén speed, k is the wavenumber and l is an integer. If $l\Omega_\alpha = s\Omega_i$ for some integer s, the thermal majority ions give additional positive energy loading through the resonant ion Bernstein wave that they support. This loading reduces the growth rate of the instability. We note that this mechanism involves collective excitation driven by all the superthermal ions — wave-particle resonance does not arise in the case of $k_\parallel = 0$.

When $k_\parallel \neq 0$, wave-particle resonance is possible, with the resonance condition given by

$$\omega = l\Omega_\alpha + k_\parallel v_\parallel \tag{11}$$

The thermal ions give resonant cyclotron damping; in the limit $k_\parallel \to 0$, this is treated as being negligible in Ref. [22], but no other mechanism that might give rise to a threshold in the absence of cyclotron damping is considered. In particular, the role of positive energy loading due to resonant thermal ion cyclotron harmonic waves is not addressed. However, in Ref. [20] the positive energy loading due to resonant cyclotron harmonic waves at $k_\parallel = 0$ is shown to be crucial. Physically, this reflects the fact that the stabilizing influence of the thermal ions ceases to act through the wave-particle resonant cyclotron damping as $k_\parallel = 0$, but acts instead through cyclotron harmonic wave–wave resonance.

5.2. Linear wave analysis of the ion cyclotron instability

We are concerned with energetic alpha particles in deuterium plasma, so that $\Omega_\alpha = \Omega_i = \Omega_D$ and $l = s$. For simplicity, we consider first the case of perpendicular propagation, where the dispersion relation has the form [19–21]

$$\frac{\omega^2 - c_A^2 k^2}{\omega^2} = A\xi \frac{\omega}{\omega - l\Omega_\alpha} + B \frac{\omega}{\omega - s\Omega_i} \tag{12}$$

plus higher order resonances. Here $\xi = n_\alpha / n_i$, where the number densities of the two ion species are n_α and n_i, and the coefficients A and B are complicated functions determined by the velocity space structure of the ion distributions; details are given in Refs [19–21]. Physically, instability arises in Eq. (12) through resonance between the fast Alfvén wave branch (left hand side) and cyclotron harmonic waves (right hand side) supported by the energetic ions (negative energy driving mechanism) and background ions (positive energy loading). Before presenting the results of a numerical solution of the full dispersion relation, it is instructive to consider the analytical approximation that arises in the limit where $\omega^2 \gg \Omega_i^2$, provided certain conditions are satisfied. If the concentration of energetic ions, the plasma beta, and the ratio c_A/c are all small, it can be shown that $\Delta\omega$ ($\equiv \omega - \omega_0$) for a monoenergetic minority ion distribution is given by (see Refs [19, 20])

$$\frac{\Delta\omega^2}{\omega_0^2} = \frac{1}{2\omega_{pi}^2} \left(\omega_{p\alpha}^2 \frac{c_A^2}{v_0^2} \chi_0^2(z_\alpha) + \omega_{pi}^2 \frac{s^2}{z_i^2} I_s(z_i^2) \exp(-z_i^2) \right) \tag{13}$$

where $\omega_{p\alpha}$ and ω_{pi} are the plasma frequencies of the two ion species, v_0 is the (unique) speed of the minority ions,

$$z_\alpha = \frac{k v_0}{\Omega_\alpha} = l \frac{v_0}{c_A} \tag{14}$$

and

$$z_i^2 = \frac{k^2 v_i^2}{2\Omega_i^2} \tag{15}$$

where v_i is the majority ion thermal speed. The function χ_0^2 is a function of z_α, which depends on the

velocity space distribution of minority ions (see below), and I_s is the modified Bessel function of the first kind of order s. The variable χ_0^2 can be positive or negative, depending on the value of z_α, whereas $I_s(z_i^2)$ is always positive. Instability occurs if the right hand side of Eq. (13) is negative, in which case the growth rate is $|\Delta\omega|$. In the limit $v_i \to 0$ we find that

$$\frac{\Delta\omega}{\omega_0} = \frac{1}{\sqrt{2}} \frac{\omega_{p\alpha}}{\omega_{pi}} \frac{l}{z_\alpha} \chi_0(z_\alpha) \tag{16}$$

In this equation we have used the second equality in Eq. (14).

5.3. Criteria for instability in JET

In Section 4.2, we saw that the large drift orbits cause the energetic ions to form a ring distribution in velocity space at the plasma edge. We have approximated the ring distribution analytically by the function $f_\alpha \propto \delta(v_\parallel)\,\delta(v_\perp - v_{\perp 0})$, from which it can be shown that

$$\chi_0^2 = z_\alpha \frac{dJ_l^2}{dz_\alpha} - \frac{2z_\alpha}{ls} \frac{d}{dz_\alpha}\left(z_\alpha J_l \frac{dJ_l}{dz_\alpha}\right) + \frac{z_\alpha}{l^2 s^2} \frac{d}{dz_\alpha}\left[z_\alpha^2 \left(\frac{dJ_l}{dz_\alpha}\right)^2\right] \tag{17}$$

where J_l is the Bessel function of order l. In the general case, we consider propagation of waves with non-zero $k_\parallel$. Limitations of space, however, prevent us from presenting a full treatment of the general dispersion relation here, although many of its features resemble those in Eq. (12), and we refer the reader elsewhere [23] for details. Using parameters appropriate for the JET PTE experiment, and assuming that the alpha particles have a ring distribution in velocity space, we find that all the cyclotron harmonics, including $l = 1$, can be unstable when $k_\parallel \neq 0$. In Fig. 18, we display simultaneous multiple cyclotron harmonic instabilities for oblique ($\theta = 85°$) and perpendicular ($\theta = 90°$) propagation. Furthermore, we find that obliquely propagating ion cyclotron waves can be unstable when the concentration of alpha particles is extremely small: except within a few degrees of the perpendicular, there is apparently no threshold concentration of minority ions below which instability cannot take place. The physical reason for this is the following. As $\xi \to 0$, the perturbation to the wave frequency arising from the energetic ions becomes arbitrarily small, so $\omega \to l\Omega_\alpha$. In fact, the negative energy driving term in the dispersion relation (represented in the case of $k_\parallel = 0$ by the first term on the right hand side of Eq. (12)) becomes independent of ξ as $\xi \to 0$. When $k_\parallel = 0$, the second (positive energy loading) term in Eq. (12) tends to infinity as $\xi \to 0$, thus suppressing the instability. However, the resonant factor in this term arises from the large argument expansion of the plasma dispersion function $Z(\zeta_s)$, the argument in question being

$$\zeta_s = \frac{\omega - s\Omega_i}{k_\parallel v_i} \tag{18}$$

Now, if $k_\parallel \neq 0$, $|\zeta_s| \to 0$ as $\omega \to s\Omega_i$, and so the small argument expansion of $Z(\zeta_s)$ is now appropriate. In this limit the positive energy loading term is also independent of ξ, and so ion cyclotron instability is possible for extremely small concentrations of minority ions, with growth rate $\gamma \propto \xi^{1/2}$ as $\xi \to 0$. Allowing for the effects of finite alpha particle Larmor radius and the poloidal asymmetry arising from the large drift orbits as discussed above, we estimate the local value of ξ to be of the order of 10^{-4} in the outer midplane edge plasma. Cyclotron damping on the thermal ions,

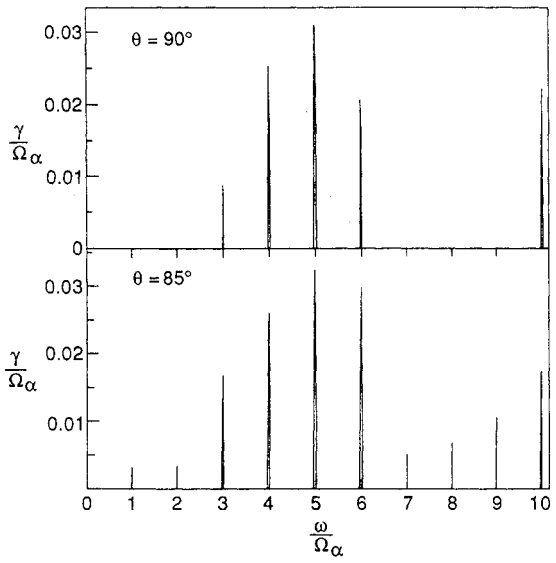

FIG. 18. Plot of the linear growth rates of alpha particle ion cyclotron harmonics using the ICI model to excite waves on the fast Alfvén cyclotron harmonic branch for propagation perpendicular to the magnetic field ($\theta = 90°$, upper diagram) and for oblique propagation ($\theta = 85°$, lower diagram). Note that all the alpha particle ion cyclotron harmonics, from $l = 1$ upwards, are linearly unstable in the oblique case. The calculation is based on a ring distribution of 3.5 MeV alpha particles and for the following JET edge plasma parameters: magnetic field B = 2.07 T, thermal ion density $n_i = 1.7 \times 10^{19}$ m^{-3}, ion temperature T = 1 keV and an alpha particle concentration ratio $n_\alpha/n_i = 1.5 \times 10^{-4}$.

which is a physical phenomenon distinct from positive energy loading, also takes place as we discussed above, but these combined effects are overcome by the driving term in the cases considered. There will be a threshold value of ξ for instability, due to the effects of electron Landau damping and transit time damping, but we expect this threshold to be extremely low.

In Section 2 it was noted that the maximum value of $k_\parallel$ for fast magnetosonic waves which can propagate in the PTE plasma is approximately 40 m^{-1}. For a fast wave resonant at the lth alpha particle ion cyclotron harmonic and propagating at an angle ϕ to the perpendicular, we have

$$k_\parallel \approx \frac{l\Omega_\alpha}{c_A} \sin\phi \approx 10\, l \sin\phi \qquad (19)$$

in the JET edge plasma. Thus we expect to detect lth harmonic radiation provided that it propagates at an angle

$$|\phi| < \sin^{-1}\left(\frac{4}{l}\right) \qquad (20)$$

The calculated propagation angles for maximum instability lie well within this range.

The present analysis omits an additional driving term (Eq. (9)) arising from the spatial inhomogeneity of the fast ion distribution at the edge of the plasma. It follows from the work of Ref. [22] that the additional operator associated with the fast ion density gradient and the primary operator associated with the velocity space gradient are in the ratio

$$\frac{\omega_{*\alpha}}{\omega} \cong \frac{k_y v_\alpha^2}{\omega\Omega_\alpha L_{n\alpha}} \cong \frac{1}{l}\frac{\rho_\alpha}{L_{n\alpha}} k_y \rho_\alpha \qquad (21)$$

Here $\omega_{*\alpha}$ is a diamagnetic frequency, k_y is the poloidal wavenumber, v_α is the velocity of the energetic ions, and $L_{n\alpha} = -(\mathrm{d}\ln n_\alpha/\mathrm{d}r)^{-1}$ is the length scale associated with the density inhomogeneity of the energetic ions. Figure 19 shows that the ratio $\rho_\alpha/L_{n\alpha}$ comes close to unity in the JET edge plasma, whereas it is to be expected that $k_y\rho_\alpha$ would be small compared with unity. It therefore follows from Eq. (21) that density inhomogeneity may enhance the instability driving term, particularly at low l values. The exact magnitude of this term depends, in general, on the nature of the mode excited and on the detailed velocity space structure of the energetic ions.

We also note that the ICI model is capable only of predicting the excitation of modes with frequencies close to the harmonics of the cyclotron frequencies of the energetic species. In pure deuterium fusion experiments [2–6], the 3 MeV fusion proton arising from

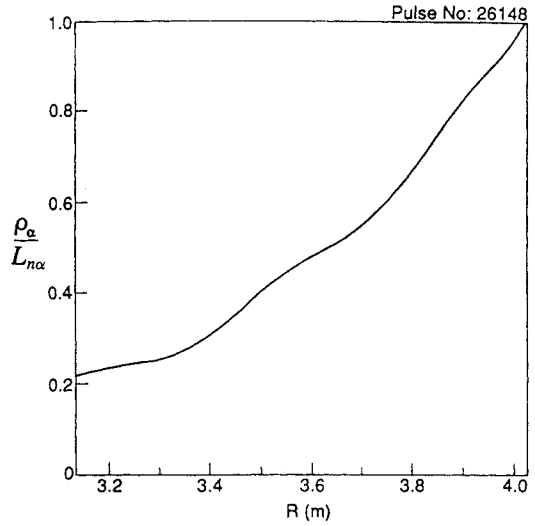

FIG. 19. Radial profile of the ratio of the alpha particle Larmor radius to the length scale of the radial alpha particle density profile, based on a TRANSP simulation of DT pulse No. 26 148 at time t = *13.2 s.*

reaction (2) is a likely candidate to drive instability. As discussed in Ref. [20], the birth velocities of the other primary fusion products in pure deuterium plasmas (see Eqs (1) and (2)) are too low to excite the ICI: $v_{birth}/c_A(R \sim 4\ \mathrm{m}) < 1$ for both ^{3}He (0.82 MeV) and T(1.0 MeV). However, we note that both the secondary protons and the secondary alpha particles (see Eqs (3) and (4)) satisfy $v_{birth}/c_A(R \sim 4\ \mathrm{m}) > 1$. The secondary alpha particles are of particular interest because, unlike the primary protons, their cyclotron harmonics contain frequencies degenerate with the odd cyclotron harmonics of deuterium $\omega \cong l\Omega_D$ ($l = 1, 3, 5, \ldots$). As noted above, for waves propagating at more than a few degrees to the perpendicular, there is no threshold in concentration below which instability cannot take place. Thus, in principle, the secondary alpha particles could excite all the deuteron harmonics observed in pure deuterium discharges. Again, the question of non-linear saturation would arise, together with the possibility of non-linear mode–mode coupling. For example, the latter could lead to equipartition of energy between modes supported by the deuterium background giving rise to similar forms of ICE spectra in pure deuterium and DT plasmas. Thus, deuterium cyclotron harmonics would be excited in a bulk deuterium plasma, irrespective of whether the driving particle is a 3 MeV primary fusion proton or a 3.6 or 3.7 MeV secondary alpha particle (in the pure deuterium case) or a 3.6 MeV primary alpha particle (in the DT case).

So far we have considered only the conditions necessary for linear growth of the ICI. The linear growth rates of different harmonics do not necessarily correlate with the intensities of the corresponding ICE lines, since it is likely that the latter are determined by a non-linear saturation process, which remains to be identified. At saturation, there are balanced energy flows into and out of the wave fields. We cannot, at present, identify the dominant channel for energy loss. However, if we suppose, for example, that saturation occurs when a certain fraction of the free energy associated with the ring population is transformed into wave energy, then a linear scaling of wave intensity with the density of fusion products would naturally follow. Such a scaling would be consistent with the experimental results of Fig. 5, which shows a nearly linear relationship between the intensity of an ICE line and the total neutron flux in the discharge.

6. DISCUSSION

We have noted fluctuations in the ICE, which are spatially coherent over a radial range $\Delta R \sim 20$ cm, and whose amplitude is of order 100%. For the plasma parameters of the JET tritium experiment, the ICI model predicts a linear growth rate of approximately 1 MHz, indicating that the mode can be switched on at a rate significantly faster than the data sampling rate of 2 kHz. The model may also be consistent with the observation of the disappearance of the ICE signal, which is correlated with the large amplitude ELMs. If a large ELM expels energetic ions from an outer plasma region of thickness approximately 30 cm, the unstable LE population will temporarily be annihilated, leading to the observed extinction of the ICE signal. However, the central birth of fusion ions continues and is sufficient to rebuild the fast ion population thus causing the instability to reappear after the ELM. The ICE signal returns after a delay, which we noted in Section 3.4.2 is approximately 20 ms. To explain this delay, we estimate the time taken to replace completely the ring of LE ions in velocity space. First, consider the time taken for alpha particles, freshly born into LE orbits, to diffuse in energy from their initial birth energy $E_{\alpha 0}$ to a final energy $E_{\alpha 0} - \Delta E_\alpha$. The decrement ΔE_α is equivalent to the energy width of the ring shown in Fig. 16: alpha particles slowing down by ion–electron collisions move radially in velocity space. The time taken for the ring to be refilled with energetic alpha particles is given by

$$\Delta t_s \approx -\ln\left(1 - \frac{\Delta E_\alpha}{E_{\alpha 0}}\right) \frac{\langle \tau_s \rangle}{2} \tag{22}$$

where $\langle \tau_s \rangle$ is the momentum slowing down time of the alpha particle due to collisions with electrons, averaged over its trapped orbit. During the period of intense large amplitude ELM activity in pulse No. 26 148, the TRANSP simulation allows us to estimate $\langle \tau_s \rangle \sim 300$ ms. Taking the energy width of the ring to be in the range $\Delta E_\alpha = 0.5$–1.0 MeV, we predict the refilling time of the ring to be in the range $\Delta t_s = 23$–50 ms, close to the observed delay. Partial filling of the ring may be sufficient to produce unstable structures in velocity space, which would form on time-scales at the lower end of this range. The ring may, however, also be replenished by pitch angle scattering of energetic alpha particles from adjacent orbits in the passing region, close to the trapped–passing boundary, as shown in Fig. 14(a). To refill the ring by this process, the passing particles would need to be scattered in pitch angle by an amount of the order of the pitch angle width of the ring, $\Delta\psi \sim 20°$. This process would take a time

$$\Delta t_{pa} \approx \left(\frac{2\Delta\psi}{\pi}\right)^2 \langle \tau_{\pi/2} \rangle \tag{23}$$

to complete, where $\langle \tau_{\pi/2} \rangle$ is the average time for an energetic alpha particle to be scattered through a pitch angle of $\pi/2$. During the period of the ELM activity in pulse No. 26 148, the TRANSP simulation gives values of $\langle \tau_{\pi/2} \rangle$ in the range 20–40 s, and a corresponding range $\Delta t_{pa} = 1$–2 s. It is thus unlikely that classical pitch angle scattering collisions can repopulate the ring on the observed time-scale of approximately 20 ms.

The observed correlation of ICE with inverted sawteeth can also be interpreted in a complementary way. Following the central sawtooth collapse, a local enhancement of fusion reactivity occurs as the heat pulse propagates outwards. In the region just exterior to the sawtooth inversion radius, the heat pulse will produce a temporary enhancement in reactivity and therefore of the LE population, resulting in a pulse of ICE correlated with the inverted sawtooth. We noted above that in the PTE series of discharges, with plasma current $I_p = 3.1$ MA, the ICE–sawtooth correlations were not as clear as those observed in the earlier series of high current discharges. This may be connected with the fact that the sawtooth inversion radius in the PTE discharges is smaller ($r/a \sim 0.33$) than in the earlier high current ohmically heated discharges ($r/a \sim 0.58$), so that the influence of sawteeth on the LE population is weaker. From MHD observations we note, in addition, that outer modes with

$m > 1$ have a relatively stronger effect on the ICE compared with central modes.

Let us now turn to an interesting null observation: the apparent absence of ICE lines from the plasma centre. If superthermal ICE is indeed driven by velocity space instability, the conditions for some form of population inversion must be satisfied in the emitting region. For example, it has been noted [6, 24, 25] that if the fusion reactivity increases sufficiently rapidly, it can generate an unstable hollow shell type fusion product distribution. However, it is unlikely that these conditions exist in the centre in the PTE plasma, since the rate of rise of the fusion reactivity R_{DT} (Fig. 7) is insufficient to satisfy the criterion for velocity space population inversion [24, 25]

$$\tau_s \frac{1}{R_{DT}} \frac{\partial R_{DT}}{\partial t} \geq 3 - \nu_{loss} \tau_s \qquad (24)$$

unless the alpha particle loss frequency ν_{loss} is significant. In the edge plasma, ν_{loss} may be sufficiently large for the inequality Eq. (24) to be satisfied; but in the plasma centre, we expect ν_{loss} to be negligible. Hence unstable shell type distributions can be generated more easily in the edge plasma than in the plasma centre. This is consistent with the fact that ICE from the plasma centre is not observed. Marginal satisfaction of Eq. (24) during the rapid heating phase allows us to place an upper limit on the value of $\nu_{loss} \sim 6\ s^{-1}$.

The width of the spectral lines is limited by the radial extent of the source region. As we have discussed, the most likely driving mechanism appears to be velocity space anisotropy arising from drift orbit excursions. Figure 17 shows that significant anisotropy is confined to the region $0.8 \leq r/a \leq 1.0$. Given the inverse dependence of local cyclotron frequency on major radius, it follows that this radial range corresponds to a frequency range

$$\Delta\nu/\nu \approx 0.2a/R_{edge} \approx 0.06 \qquad (25)$$

which is close to the observed spectral linewidth $\Delta\nu/\nu \approx 0.09$. The small size of the difference between the observed linewidth and that obtained from Eq. (25) places a constraint on the magnitude of any additional line broadening mechanism.

The fine structure of the low l ICE lines is a new feature of the present observations. We recall from Section 3.1 that the lines are split into blended doublet or triplet shapes with linewidth $\Delta\nu/\nu \sim 0.06$. This may be due to poloidal field or diamagnetic effects. Adam and Jacquinot [26] have examined the fine structure of global fast wave modes in a tokamak, which arises from the interaction of the poloidal field with the toroidal plasma current. This effect produces a small energy shift between co-propagating and counter-propagating waves. The magnitude of the splitting, $\Delta n_\parallel \sim (c/\omega r)(B_\theta/B)$, corresponds to $\Delta k_\parallel \sim 0.1\ m^{-1}$ in the present case. Given the typical acceptance range of the JET antenna, it is clear that $\Delta k_\parallel/|k_\parallel| \sim \Delta\nu/\nu \sim 0.06$ would be compatible with existing data. We also note that this frequency splitting is comparable in magnitude with the inhomogeneity drift frequency of the energetic ions, ω_{di}, suggesting that the superposition of collective modes with relative frequencies $\pm\omega_{di}$ may be responsible. For radially localized modes of the type discussed in Ref. [22], this term can be interpreted as referring to the two waves (travelling in the $\pm z$ directions) needed to form the mode. As l increases, the splitting also increases, and the lines eventually overlap at sufficiently large l, forming a continuum. Complete overlap of the lines would occur for $l > 6$, corresponding to frequencies in excess of 100 MHz, and coinciding with the band of ICE continua observed in JET and TFTR experiments.

It is instructive to consider how the maximum radial displacement of each of the pure deuterium fusion products scales with initial perpendicular energy, $E_{\perp 0}$. The maximum minor radial excursion is given by $r_{max} \propto \rho_\theta^{2/3} \propto (A_\alpha E_{\perp 0})^{1/3}/Z_\alpha^{2/3}$, where ρ_θ is the poloidal Larmor radius, and A_α and Z_α are the atomic mass and atomic number of the fusion product. For the set of pure deuterium fusion products {proton (3 MeV), triton (1 MeV), ^{3}He (0.82 MeV)}, we calculate the set of ratios

$$r_{max}(\text{DD product})/r_{max}(3.6\ \text{MeV alpha particle})$$

to be {0.95, 0.95, 0.56}. This shows that it is possible only for the protons and tritons to follow LE orbits; the ^{3}He ions have insufficient birth energy to reach the JET plasma edge. We recall that ICE lines with frequencies at ^{3}He cyclotron harmonics have been observed in TFTR experiments, but not in JET. The larger poloidal Larmor radii expected in TFTR, which has a lower plasma current than JET, may allow the ^{3}He fusion ions to reach the edge plasma and give rise to the observed ^{3}He ICE lines.

The present ICE results are also of interest in the context of current theoretical investigations of collective alpha particle instabilities, in particular, the toroidicity induced Alfvén eigenmodes (TAEs) [27, 28]. The TAEs are discrete MHD modes appearing near the Alfvén frequency, which can be resonantly destabilized by circulating and trapped alpha particles when the alpha particle radial pressure gradient is sufficiently steep and β_α is sufficiently large. In the

DT pulse No. 26 148, the predicted TAE mode frequency is in the range 100–300 kHz. It has been suggested that excitation of such modes can lead to loss or radial redistribution of the energetic ions. The theoretical boundary for the destabilization of TAE modes has been computed for realistic tokamak conditions [29] and depends primarily on the magnitude of the volume averaged toroidal beta, $\langle\beta_\alpha\rangle$, and the ratio $v_{\alpha 0}/c_A$. Details of the TAE threshold also depend on the ratio of the length scale of the alpha particle pressure, $L_\alpha = -(\mathrm{d} \ln \beta_\alpha/\mathrm{d}r)^{-1}$ to the plasma minor radius, a. From the theoretical literature we note, however, that there is considerable uncertainty in the precise location of the instability boundary. Using the TRANSP Monte Carlo alpha particle results for DT pulse No. 26 148 (at a time of 13.2 s, near the peak of the DT fusion production), we find maximum values of $L_\alpha/a \sim 0.35$, $v_{\alpha 0}/c_A \sim 1.8$ and $\langle\beta_\alpha\rangle \cong 1.36 \times 10^{-4}$. These values have been compared with the theoretical TAE instability boundary [12], showing the JET data to lie marginally in the stable region. This is due, primarily, to the large ratio of $v_{\alpha 0}/c_A$. Values of this ratio closer to unity would have implied instability. This result is consistent with the observation that the integrated ICE signal in this discharge (Fig. 8) simply increases in proportion to the calculated alpha particle density up to the time of the X event. There is no evidence for saturation in the ICE signal that might have been attributable to anomalous alpha particle losses.

The origin of the MHD mode shown in Fig. 11 is unknown. Although it preceeds the ELM, it is not typical of other ELM precursors that have been observed [14]. However, the low frequency of this mode (4.5 kHz) makes it unlikely to be of TAE or fishbone type. The fact that this mode has been observed only in the two DT discharges (pulse Nos 26 147 and 26 148) where its destabilization coincides with the growth of the ICE signal, might indicate that it is triggered by fusion alpha particles. Future DT experiments will enable us to test this hypothesis.

Finally, we note that superthermal emission at sequential multiple cyclotron harmonics of a diffuse, ring or shell type energetic ion population has also been observed in space plasmas; see, for example, Ref. [30]. The ICI model adopted in the present paper also provides a candidate emission mechanism in this case [31].

7. CONCLUSIONS

In this paper, we have reported measurements of ICE made during the first tritium experiments on JET. The spectra contain superthermal, narrow, equally spaced emission lines that correspond to successive cyclotron harmonics of deuterons or alpha particles at the outer midplane edge of the plasma, near the last closed flux surface. At frequencies above approximately 100 MHz, corresponding to the sixth or seventh alpha particle ion cyclotron harmonic, the individual emission lines merge into a broad continuum. The ICE spectra have similar forms in pure deuterium and in mixed DT discharges. On changing the gas feed to the neutral beam injectors from pure deuterium to a mixture of deuterium and tritium at constant injected power, the ICE intensity increased in proportion to the neutron flux. Thus, fusion alpha particles — and not the injected beam ions — provide the free energy to generate ICE.

In pure deuterium and mixed DT JET discharges, the time averaged ICE power increases linearly with the total neutron flux over a range of six decades in signal intensity. The ICE signal vanishes whenever a large amplitude edge localized MHD mode (ELM) occurs. Such ELMs penetrate sufficiently deeply into the plasma to extinguish the ICE source by releasing energetic ions from the edge localized emitting region, which is inferred from frequency matching considerations. During a single time evolving DT discharge, the rise and fall of the neutron flux is closely followed by that of the ICE intensity, which lags by a time of the order of the alpha particle slowing down time. Calculations with the TRANSP Monte Carlo code show a similar time lag for the buildup of the alpha particle population. Detailed single particle drift orbit calculations reveal the existence of a distinct class of fusion products, born into trapped orbits in the plasma core, which make sufficiently large orbital excursions to reach the outer midplane edge. Their presence there results in a velocity distribution for the energetic particles that is anisotropic, is not monotonically decreasing and has a ring structure. The ring is found to be linearly unstable against collective excitation of obliquely propagating waves on the fast Alfvén-ion Bernstein branch at all ion cyclotron harmonics.

This paper has described the first measurements of ion cyclotron emission from confined, energetic alpha particles in a tokamak fusion experiment using deuterium–tritium fuel. It is clear that ICE possesses unique potential as a diagnostic for fusion alpha particles; no other diagnostic system has performed this

role in the first tritium experiments on JET. However, the full exploitation of ICE will require further developments in theoretical interpretation, particularly in the calculation of the non-linear saturated amplitude of the ICI mode and its relation to the observed ICE intensity.

ACKNOWLEDGEMENTS

It is a pleasure to thank the many JET Team members involved in the PTE experimental campaign from the Operations, Heating and Diagnostic groups. We also thank Andy Sibley and Martin Schmid for technical advice, Piet van Belle for help with running the JET single particle orbit code, Bernard Balet and Pam Stubberfield for their help with the TRANSP alpha particle Monte Carlo code, Duarte Borba and Shakeib Ali-Arshad for help with MHD analysis, and Jim Hastie and Chris Lashmore-Davies for helpful discussions.

REFERENCES

[1] JET TEAM, The JET Project — Design Proposal, Rep. EUR-JET-R5, CEC, Brussels (1975).
[2] COTTRELL, G.A., et al., in Controlled Fusion and Plasma Heating (Proc. 13th Eur. Conf. Schliersee, 1986), Vol. 10C, Part II, European Physical Society, Geneva (1986) 37.
[3] CLARK, W.H.M., in Heating in Toroidal Plasmas (Proc. 4th Int. Symp. Rome, 1984), Vol. 1, Monotypia Franchi, Città di Castello (Perugia) (1984) 385.
[4] COTTRELL, G.A., in Applications of RF Waves to Tokamak Plasmas (Proc. Course and Workshop Varenna, 1985), Vol. 2, CEC, Brussels (1985) 710.
[5] COTTRELL, G.A., DENDY, R.O., Phys. Rev. Lett. **60** (1988) 33.
[6] SCHILD, P., et al., Nucl. Fusion **29** (1989) 834.
[7] GREENE, G.J., TFTR GROUP, in Controlled Fusion and Plasma Heating (Proc. 17th Eur. Conf. Amsterdam, 1990), Vol. 14B, Part IV, European Physical Society, Geneva (1990) 1540.
[8] YOUNG, K., TFTR Group, Princeton University, Plasma Physics Laboratory, Princeton, NJ, personal communication, 1992.
[9] JET TEAM, Nucl. Fusion **32** (1992) 187.
[10] COTTRELL, G.A., et al., in Controlled Fusion and Plasma Physics (Proc. 19th Int. Conf. Innsbruck, 1992), Vol. 16C, Part I (1992) 327.
[11] GOLDSTON, R.J., et al., J. Comput. Phys. **43** (1981) 61.
[12] BALET, B., et al., Nucl. Fusion **33** (1993) 1345.
[13] REICHLE, R., et al., Termination of High Performance Discharges in JET (in preparation).
[14] ALI-ARSHAD, S., et al., in Controlled Fusion and Plasma Physics (Proc. 19th Int. Conf. Innsbruck, 1992), Vol. 16C, Part I, European Physical Society, Geneva (1992) 227.
[15] BATCHELOR, D.B., et al., Phys. Fluids B **1** (1989) 1174.
[16] VAN BELLE, P., JET, personal communication, 1992.
[17] STRINGER, T.E., Plasma Phys. **16** (1974) 651.
[18] MIKHAILOVSKII, A.B., in Reviews of Plasma Physics, Vol. 9 (LEONTOVICH, M.A., Ed.), Consultants Bureau, New York (1986) 103.
[19] BELIKOV, V.S., KOLESNICHENKO, Ya.I., Sov. Phys. — Tech. Phys. **20** (1976) 1146.
[20] DENDY, R.O., et al., Phys. Fluids B **4** (1992) 3996.
[21] DENDY, R.O., et al., Phys. Fluids B **5** (1993) 1937.
[22] COPPI, B., et al., Phys. Fluids **29** (1986) 4060.
[23] DENDY, R.O., et al., (in preparation).
[24] SIGMAR, D.J., in Physics of Plasmas Close to Thermonuclear Conditions (Proc. Course Varenna, 1979), Vol. 1, CEC, Brussels (1980) 271.
[25] CORDEY, J.G., et al., Nucl. Fusion **21** (1981) 581.
[26] ADAM, J., JACQUINOT, J., Eigenmode Field Structure of the Fast Magnetosonic Wave, Rep. EUR-CEA-FC-886, Association Euratom-CEA sur la Fusion, Fontenay-aux-Roses, France.
[27] CHEN, L., in Theory of Fusion Plasmas (Proc. Course Varenna–Lausanne Int. Workshop Chexbres, 1988), Editrice Compositori, Bologna (1988) 327.
[28] CHENG, C.Z., Phys. Fluids B **3** (1991) 2463 and references therein.
[29] BUDNY, R.V., et al., Nucl. Fusion **32** (1992) 429.
[30] PERRAUT, S., et al., J. Geophys. Res. **87** (1982) 6219.
[31] McCLEMENTS, K.G., DENDY, R.O., J. Geophys. Res. **98** (1993) 11 689.

(Manuscript received 10 December 1992,
Final manuscript received 26 April 1993)